

<sup>1</sup> Geometric models reveal behavioral and neural  
<sup>2</sup> signatures of transforming naturalistic experiences into  
<sup>3</sup> episodic memories

<sup>4</sup> Andrew C. Heusser<sup>1, 2, †</sup>, Paxton C. Fitzpatrick<sup>1, †</sup>, and Jeremy R. Manning<sup>1, \*</sup>

<sup>1</sup>Department of Psychological and Brain Sciences

Dartmouth College, Hanover, NH 03755, USA

<sup>2</sup>Akili Interactive Labs

Boston, MA 02110

<sup>†</sup>Denotes equal contribution

<sup>\*</sup>Corresponding author: Jeremy.R.Manning@Dartmouth.edu

<sup>5</sup> October 9, 2020

## Abstract

7        The mental contexts in which we interpret experiences are often person-specific, even when  
 8        the experiences themselves are shared. We developed a geometric framework for mathematically  
 9        characterizing the subjective conceptual content of dynamic naturalistic experiences. We model  
 10      experiences and memories as *trajectories* through word embedding spaces whose coordinates  
 11      reflect the universe of thoughts under consideration. Memory encoding can then be modeled  
 12      as geometrically preserving or distorting the *shape* of the original experience. We applied our  
 13      approach to data collected as participants watched and verbally recounted a television episode  
 14      while undergoing functional neuroimaging. Participants' recounts all preserved coarse spatial  
 15      properties (essential narrative elements), but not fine spatial scale (low-level) details, of the  
 16      episode's trajectory. We also identified networks of brain structures sensitive to these trajectory  
 17      shapes. Our work provides insights into how we preserve and distort our ongoing experiences  
 18      when we encode them into episodic memories.

## 19      Introduction

20     What does it mean to *remember* something? In traditional episodic memory experiments (e.g., list-  
 21     learning or trial-based experiments; Kahana, 1996; Murdock, 1962), remembering is often cast as a  
 22     discrete, binary operation: each studied item may be separated from the rest of one's experience and  
 23     labeled as having been either recalled or forgotten. More nuanced studies might incorporate self-  
 24     reported confidence measures as a proxy for memory strength, or ask participants to discriminate  
 25     between recollecting the (contextual) details of an experience and having a general feeling of  
 26     familiarity (Yonelinas, 2002). Using well-controlled, trial-based experimental designs, the field  
 27     has amassed a wealth of information regarding human episodic memory (for review see Kahana,  
 28     2012). However, there are fundamental properties of the external world and our memories that  
 29     trial-based experiments are not well suited to capture (for review, also see Huk et al., 2018; Koriat  
 30     and Goldsmith, 1994). First, our experiences and memories are continuous, rather than discrete—  
 31     isolating a naturalistic event from the context in which it occurs can substantially change its  
 32     meaning. Second, whether or not the rememberer has precisely reproduced a specific set of words

33 in describing a given experience is nearly orthogonal to how well they were actually able to  
34 remember it. In classic (e.g., list-learning) memory studies, by contrast, the number or proportion  
35 of *exact* recalls is often considered to be a primary metric for assessing the quality of participants'  
36 memories. Third, one might remember the essence (or a general summary) of an experience but  
37 forget (or neglect to recount) particular low-level details. Capturing the essence of what happened  
38 is often a main goal of recounting an episodic memory to a listener, whereas the inclusion of specific  
39 low-level details is often less pertinent.

40 How might we formally characterize the *essence* of an experience, and whether it has been  
41 recovered by the rememberer? And how might we distinguish an experience's overarching essence  
42 from its low-level details? One approach is to start by considering some fundamental properties  
43 of the dynamics of our experiences. Each given moment of an experience tends to derive meaning  
44 from surrounding moments, as well as from longer-range temporal associations (Lerner et al., 2011;  
45 Manning, 2019, 2020). Therefore, the timecourse describing how an event unfolds is fundamental  
46 to its overall meaning. Further, this hierarchy formed by our subjective experiences at different  
47 timescales defines a *context* for each new moment (e.g., Howard and Kahana, 2002; Howard  
48 et al., 2014), and plays an important role in how we interpret that moment and remember it  
49 later (for review see Manning, 2020; Manning et al., 2015). Our memory systems can leverage  
50 these associations to form predictions that help guide our behaviors (Ranganath and Ritchey,  
51 2012). For example, as we navigate the world, the features of our subjective experiences tend  
52 to change gradually (e.g., the room or situation we find ourselves in at any given moment is  
53 strongly temporally autocorrelated), allowing us to form stable estimates of our current situation  
54 and behave accordingly (Zacks et al., 2007; Zwaan and Radvansky, 1998).

55 Occasionally, this gradual drift of our ongoing experience is punctuated by sudden changes, or  
56 shifts (e.g., when we walk through a doorway; Radvansky and Zacks, 2017). Prior research suggests  
57 that these sharp transitions (termed *event boundaries*) help to discretize our experiences (and their  
58 mental representations) into *events* (Brunec et al., 2018; Clewett and Davachi, 2017; DuBrow and  
59 Davachi, 2013; Ezzyat and Davachi, 2011; Heusser et al., 2018a; Radvansky and Zacks, 2017). The  
60 interplay between the stable (within-event) and transient (across-event) temporal dynamics of an

experience also provides a potential framework for transforming experiences into memories that distills those experiences down to their essences. For example, prior work has shown that event boundaries can influence how we learn sequences of items (DuBrow and Davachi, 2013; Heusser et al., 2018a), navigate (Brunec et al., 2018), and remember and understand narratives (Ezzyat and Davachi, 2011; Zwaan and Radvansky, 1998). This work also suggests a means of distinguishing the essence of an experience from its low-level details: The overall structure of events and event transitions reflects how the high-level experience unfolds (i.e., its essence), while subtler event-level properties reflect its low-level details. Prior research has also implicated a network of brain regions (including the hippocampus and the medial prefrontal cortex) in playing a critical role in transforming experiences into structured and consolidated memories (Tompry and Davachi, 2017).

Here, we sought to examine how the temporal dynamics of a naturalistic experience were later reflected in participants' memories. We also sought to leverage the above conceptual insights into the distinctions between an experience's essence and its low-level details to build models that explicitly quantified these distinctions. We analyzed an open dataset that comprised behavioral and functional Magnetic Resonance Imaging (fMRI) data collected as participants viewed and then verbally recounted an episode of the BBC television show *Sherlock* (Chen et al., 2017). We developed a computational framework for characterizing the temporal dynamics of the moment-by-moment content of the episode and of participants' verbal recalls. Our framework uses topic modeling (Blei et al., 2003) to characterize the thematic conceptual (semantic) content present in each moment of the episode and recalls by projecting each moment into a word embedding space. We then use hidden Markov models (Baldassano et al., 2017; Rabiner, 1989) to discretize this evolving semantic content into events. In this way, we cast both naturalistic experiences and memories of those experiences as geometric *trajectories* through word embedding space that describe how they evolve over time. Under this framework, successful remembering entails verbally traversing the content trajectory of the episode, thereby reproducing the shape (essence) of the original experience. Our framework captures the episode's essence in the sequence of geometric coordinates for its events, and its low-level details by examining its within-event geometric properties.

89 Comparing the overall shapes of the topic trajectories for the episode and participants' recalls  
90 reveals which aspects of the episode's essence were preserved (or lost) in the translation into  
91 memory. We also develop two metrics for assessing participants' memories for low-level details:  
92 (1) the *precision* with which a participant recounts details about each event, and (2) the *distinctiveness*  
93 of their recall for each event, relative to other events. We examine how these metrics relate to overall  
94 memory performance as judged by third-party human annotators. We also compare and contrast  
95 our general approach to studying memory for naturalistic experiences with standard metrics for  
96 assessing performance on more traditional memory tasks, such as list-learning. Last, we leverage  
97 our framework to identify networks of brain structures whose responses (as participants watched  
98 the episode) reflected the temporal dynamics of the episode and/or how participants would later  
99 recount it.

## 100 Results

101 To characterize the dynamic content of the *Sherlock* episode and participants' subsequent recounts  
102ings, we used a topic model (Blei et al., 2003) to discover the episode's latent themes. Topic models  
103 take as inputs a vocabulary of words to consider and a collection of text documents, and return  
104 two output matrices. The first of these is a *topics matrix* whose rows are *topics* (or latent themes)  
105 and whose columns correspond to words in the vocabulary. The entries in the topics matrix  
106 reflect how each word in the vocabulary is weighted by each discovered topic. For example, a  
107 detective-themed topic might weight heavily on words like "crime," and "search." The second  
108 output is a *topic proportions matrix* with one row per document and one column per topic. The topic  
109 proportions matrix describes the mixture of discovered topics reflected in each document.

110 Chen et al. (2017) collected hand-annotated information about each of 1,000 (manually delin-  
111 eated) time segments spanning the roughly 50 minute video used in their study. Each annotation  
112 included: a brief narrative description of what was happening, the location where the action took  
113 place, the names of any characters on the screen, and other similar details (for a full list of anno-  
114 tated features, see *Methods*). We took the union of all unique words (excluding stop words, such

as “and,” “or,” “but,” etc.) across all features from all annotations as the vocabulary for the topic model. We then concatenated the sets of words across all features contained in overlapping sliding windows of (up to) 50 annotations, and treated each window as a single document for the purpose of fitting the topic model. Next, we fit a topic model with (up to)  $K = 100$  topics to this collection of documents. We found that 32 unique topics (with non-zero weights) were sufficient to describe the time-varying content of the episode (see *Methods*; Figs. 1, S2). We note that our approach is similar in some respects to Dynamic Topic Models (Blei and Lafferty, 2006) in that we sought to characterize how the thematic content of the episode evolved over time. However, whereas Dynamic Topic Models are designed to characterize how the properties of *collections* of documents change over time, our sliding window approach allows us to examine the topic dynamics within a single document (or video). Specifically, our approach yielded (via the topic proportions matrix) a single *topic vector* for each sliding window of annotations transformed by the topic model. We then stretched (interpolated) the resulting windows-by-topics matrix to match the time series of the 1,976 fMRI volumes collected as participants viewed the episode.

The 32 topics we found were heavily character-focused (i.e., the top-weighted word in each topic was nearly always a character) and could be roughly divided into themes centered around Sherlock Holmes (the titular character), John Watson (Sherlock’s close confidant and assistant), supporting characters (e.g., Inspector Lestrade, Sergeant Donovan, or Sherlock’s brother Mycroft), or the interactions between various groupings of these characters (Fig. S2). This likely follows from the frequency with which these terms appeared in the episode annotations. Several of the identified topics were highly similar, which we hypothesized might allow us to distinguish between subtle narrative differences if the distinctions between those overlapping topics were meaningful. The topic vectors for each timepoint were also *sparse*, in that only a small number of topics (typically one or two) tended to be “active” in any given timepoint (Fig. 2A). Further, the dynamics of the topic activations appeared to exhibit *persistence* (i.e., given that a topic was active in one timepoint, it was likely to be active in the following timepoint) along with *occasional rapid changes* (i.e., occasionally topic weights would change abruptly from one timepoint to the next). These two properties of the topic dynamics may be seen in the block diagonal structure of the timepoint-by-timepoint

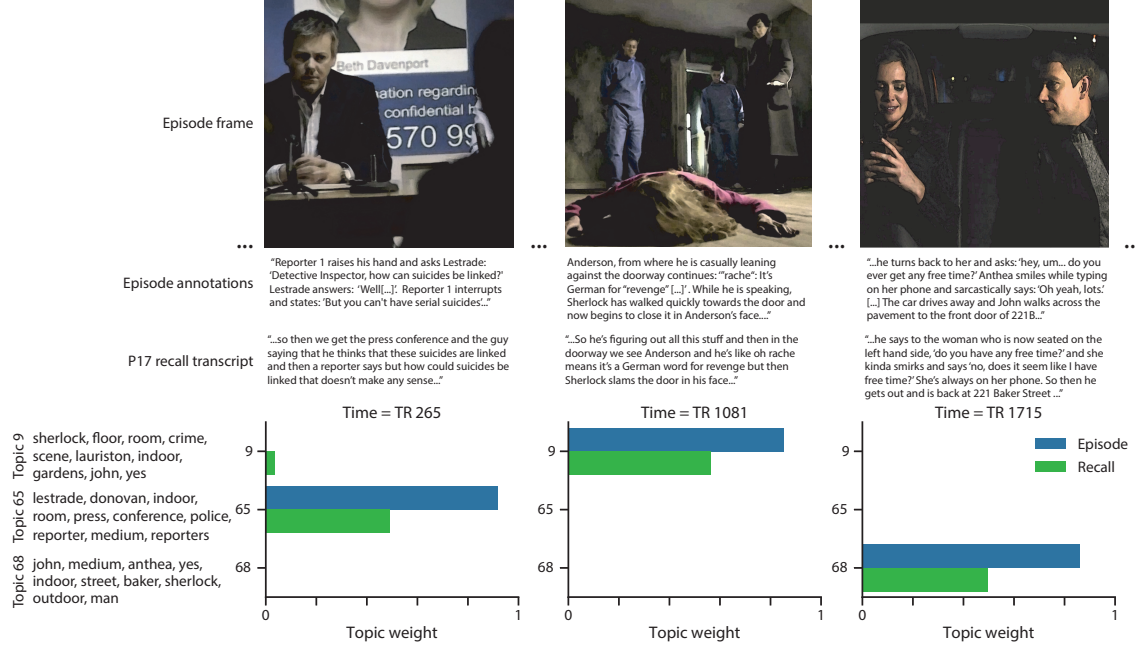


**Figure 1: Topic weights in episode and recall content.** We used detailed, hand-generated annotations describing each manually identified time segment from the episode to fit a topic model. Three example frames from the episode (first row) are displayed, along with their descriptions from the corresponding episode annotation (second row) and an example participant’s recall transcript (third row). We used the topic model (fit to the episode annotations) to estimate topic vectors for each moment of the episode and each sentence of participants’ recalls. Example topic vectors are displayed in the bottom row (blue: episode annotations; green: example participant’s recalls). Three topic dimensions are shown (the highest-weighted topics for each of the three example scenes, respectively), along with the 10 highest-weighted words for each topic. Figure S2 provides a full list of the top 10 words from each of the discovered topics.

correlation matrix (Fig. 2B) and reflect the gradual drift and sudden shifts fundamental to the temporal dynamics of many real-world experiences, as well as television episodes. Given this observation, we adapted an approach devised by Baldassano et al. (2017), and used a hidden Markov model (HMM) to identify the *event boundaries* where the topic activations changed rapidly (i.e., the boundaries of the blocks in the temporal correlation matrix; event boundaries identified by the HMM are outlined in yellow in Fig. 2B). Part of our model fitting procedure required selecting an appropriate number of events into which the topic trajectory should be segmented. To accomplish this, we used an optimization procedure that maximized the difference between the topic weights for timepoints within an event versus timepoints across multiple events (see *Methods*). We then created a stable summary of the content within each episode event by averaging the topic vectors across the timepoints spanned by each event (Fig. 2C).

Given that the time-varying content of the episode could be segmented cleanly into discrete events, we wondered whether participants' recalls of the episode also displayed a similar structure. We applied the same topic model (already trained on the episode annotations) to each participant's recalls. Analogously to how we parsed the time-varying content of the episode, to obtain similar estimates for each participant's recall transcript, we treated each overlapping window of (up to) 10 sentences from their transcript as a document, and computed the most probable mix of topics reflected in each timepoint's sentences. This yielded, for each participant, a number-of-windows by number-of-topics topic proportions matrix that characterized how the topics identified in the original episode were reflected in the participant's recalls. An important feature of our approach is that it allows us to compare participants' recalls to events from the original episode, despite that different participants used widely varying language to describe the events, and that those descriptions often diverged in content, quality, and quantity from the episode annotations. This ability to match up conceptually related text that differs in specific vocabulary, detail, and length is an important benefit of projecting the episode and recalls into a shared topic space. An example topic proportions matrix from one participant's recalls is shown in Figure 2D.

Although the example participant's recall topic proportions matrix has some visual similarity to the episode topic proportions matrix, the time-varying topic proportions for the example par-



**Figure 2: Modeling naturalistic stimuli and recalls.** All panels: darker colors indicate greater values; range: [0, 1]. **A.** Topic vectors ( $K = 100$ ) for each of the 1976 episode timepoints. **B.** Timepoint-by-timepoint correlation matrix of the topic vectors displayed in Panel A. Event boundaries discovered by the HMM are denoted in yellow (30 events detected). **C.** Average topic vectors for each of the 30 episode events. **D.** Topic vectors for each of 265 sliding windows of sentences spoken by an example participant while recalling the episode. **E.** Timepoint-by-timepoint correlation matrix of the topic vectors displayed in Panel D. Event boundaries detected by the HMM are denoted in yellow (22 events detected). For similar plots for all participants, see Figure S4. **F.** Average topic vectors for each of the 22 recall events from the example participant. **G.** Correlations between the topic vectors for every pair of episode events (Panel C) and recall events (from the example participant; Panel F). For similar plots for all participants, see Figure S5. **H.** Average correlations between each pair of episode events and recall events (across all 17 participants). To create the figure, each recalled event was assigned to the episode event with the most correlated topic vector (yellow boxes in panels G and H).

ticipant's recalls are not as sparse as those for the episode (compare Figs. 2A and D). Similarly, although there do appear to be periods of stability in the recall topic dynamics (i.e., most topics are active or inactive over contiguous blocks of time), the changes in topic activations that define event boundaries appear less clearly delineated in participants' recalls than in the episode's annotations. To examine these patterns in detail, we computed the timepoint-by-timepoint correlation matrix for the example participant's recall topic proportions matrix (Fig. 2E). As in the episode correlation matrix (Fig. 2B), the example participant's recall correlation matrix has a strong block diagonal structure, indicating that their recalls are discretized into separated events. We used the same HMM-based optimization procedure that we had applied to the episode's topic proportions matrix (see *Methods*) to estimate an analogous set of event boundaries in the participant's recounting of the episode (outlined in yellow). We carried out this analysis on all 17 participants' recall topic proportions matrices (Fig. S4).

Two clear patterns emerged from this set of analyses. First, although every individual participant's recalls could be segmented into discrete events (i.e., every individual participant's recall correlation matrix exhibited clear block diagonal structure; Fig. S4), each participant appeared to have a unique *recall resolution*, reflected in the sizes of those blocks. While some participants' recall topic proportions segmented into just a few events (e.g., Participants P4, P5, and P7), others' segmented into many shorter-duration events (e.g., Participants P12, P13, and P17). This suggests that different participants may be recalling the episode with different levels of detail—i.e., some might recount only high-level essential plot details, whereas others might recount low-level details instead (or in addition). The second clear pattern present in every individual participant's recall correlation matrix was that, unlike in the episode correlation matrix, there were substantial off-diagonal correlations. One potential explanation for this finding is that the topic models, trained only on episode annotations, do not capture topic proportions in participants' "held-out" recalls as accurately. A second possibility is that, whereas each event in the original episode was (largely) separable from the others (Fig. 2B), in transforming those separable events into memory, participants appeared to be integrating across multiple events, blending elements of previously recalled and not-yet-recalled content into each newly recalled event (Figs. 2E, S4; also see Howard et al.,

<sup>199</sup> 2012; Manning, 2019; Manning et al., 2011).

<sup>200</sup> The above results demonstrate that topic models capture the dynamic conceptual content of  
<sup>201</sup> the episode and participants' recalls of the episode. Further, the episode and recalls exhibit event  
<sup>202</sup> boundaries that can be identified automatically using HMMs to segment the dynamic content.  
<sup>203</sup> Next, we asked whether some correspondence might be made between the specific content of the  
<sup>204</sup> events the participants experienced while viewing the episode, and the events they later recalled.  
<sup>205</sup> We labeled each recall event as matching the episode event with the most similar (i.e., most highly  
<sup>206</sup> correlated) topic vector (Figs. 2G, S5). This yielded a sequence of "presented" events from the  
<sup>207</sup> original episode, and a (potentially differently ordered) sequence of "recalled" events for each  
<sup>208</sup> participant. Analogous to classic list-learning studies, we can then examine participants' recall  
<sup>209</sup> sequences by asking which events they tended to recall first (probability of first recall; Fig. 3A;  
<sup>210</sup> Atkinson and Shiffrin, 1968; Postman and Phillips, 1965; Welch and Burnett, 1924); how participants  
<sup>211</sup> most often transitioned between recalls of the events as a function of the temporal distance between  
<sup>212</sup> them (lag-conditional response probability; Fig. 3B; Kahana, 1996); and which events they were  
<sup>213</sup> likely to remember overall (serial position recall analyses; Fig. 3C; Murdock, 1962). Some of the  
<sup>214</sup> patterns we observed appeared to be similar to classic effects from the list-learning literature.  
<sup>215</sup> For example, participants had a higher probability of initiating recall with early events (Fig. 3A)  
<sup>216</sup> and a higher probability of transitioning to neighboring events with an asymmetric forward bias  
<sup>217</sup> (Fig. 3B). However, unlike what is typically observed in list-learning studies, we did not observe  
<sup>218</sup> patterns comparable to the primacy or recency serial position effects (Fig. 3C). We hypothesized  
<sup>219</sup> that participants might be leveraging meaningful narrative associations and references over long  
<sup>220</sup> timescales throughout the episode.

<sup>221</sup> Clustering scores are often used by memory researchers to characterize how people organize  
<sup>222</sup> their memories of words on a studied list (for review, see Polyn et al., 2009). We defined analogous  
<sup>223</sup> measures to characterize how participants organized their memories for episodic events (see  
<sup>224</sup> *Methods* for details). Temporal clustering refers to the extent to which participants group their recall  
<sup>225</sup> responses according to encoding position. Overall, we found that sequentially viewed episode  
events tended to appear nearby in participants' recall event sequences (mean clustering score: 0.732,

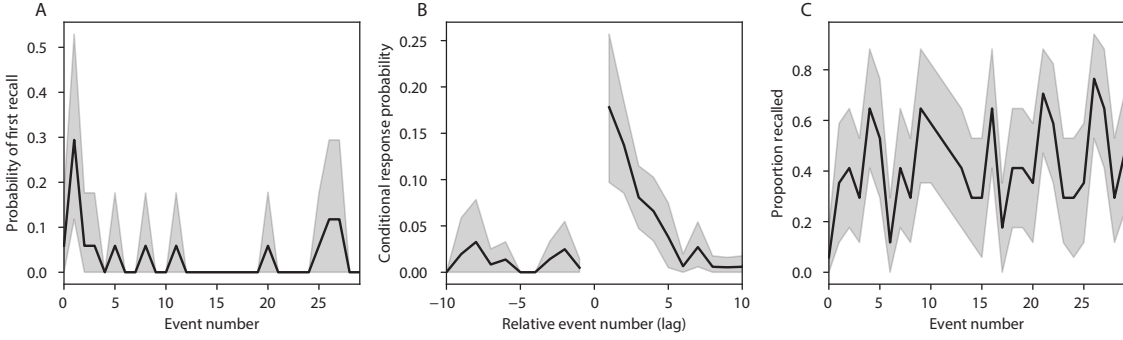


**Figure 3: Naturalistic extensions of classic list-learning memory analyses.** **A.** The probability of first recall as a function of the serial position of the event in the episode. **B.** The probability of recalling each event, conditioned on having most recently recalled the event *lag* events away in the episode. **C.** The proportion of participants who recalled each event, as a function of the serial position of the events in the episode. All panels: error ribbons denote bootstrap-estimated standard error of the mean.

227 SEM: 0.033). Participants with higher temporal clustering scores tended to exhibit better overall  
 228 memory for the episode, according to both Chen et al. (2017)'s hand-counted numbers of recalled  
 229 scenes from the episode (Pearson's  $r(15) = 0.49, p = 0.046$ ) and the numbers of episode events that  
 230 best-matched at least one recall event (i.e., model-estimated number of events recalled; Pearson's  
 231  $r(15) = 0.59, p = 0.013$ ). Semantic clustering measures the extent to which participants cluster  
 232 their recall responses according to semantic similarity. We found that participants tended to recall  
 233 semantically similar episode events together (mean clustering score: 0.650, SEM: 0.032), and that  
 234 semantic clustering score was also related to both hand-counted (Pearson's  $r(15) = 0.65, p = 0.005$ )  
 235 and model-estimated (Pearson's  $r(15) = 0.58, p = 0.015$ ) numbers of recalled events.

236 The above analyses illustrate how our framework for characterizing the dynamic conceptual  
 237 content of naturalistic episodes enables us to carry out analyses that have traditionally been  
 238 applied to much simpler list-learning paradigms. However, perhaps the most interesting aspects  
 239 of memory for naturalistic episodes are those that have no list-learning analogs. The nuances of  
 240 how one's memory for an event might capture some details, yet distort or neglect others, is central  
 241 to how we use our memory systems in daily life. Yet when researchers study memory in highly  
 242 simplified paradigms, those nuances are not typically observable. We next developed two novel,  
 243 continuous metrics, termed *precision* and *distinctiveness*, aimed at characterizing distortions in the

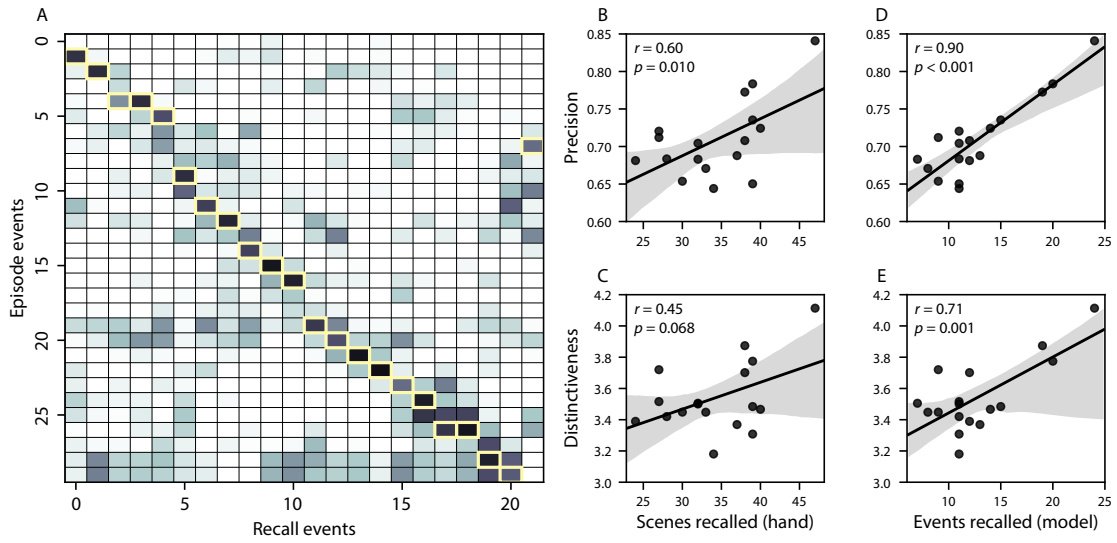


**Figure 4: Novel content-based metrics of naturalistic memory: precision and distinctiveness.** **A.** The episode-recall correlation matrix for a representative participant (P17). The yellow boxes highlight the maximum correlation in each column. The example participant’s overall precision score was computed as the average across the (Fisher z-transformed) correlation values in the yellow boxes. Their distinctiveness score was computed as the average (over recall events) of the z-scored (within column) event precisions. **B.** The (Pearson’s) correlation between precision and hand-counted number of recalled scenes. **C.** The correlation between distinctiveness and hand-counted number of recalled scenes. **D.** The correlation between precision and the number of recalled episode events, as determined by our model. **E.** The correlation between distinctiveness and the number of recalled episode events, as determined by our model.

244 conceptual content of individual recall events, and the conceptual overlap between how people  
245 described different events.

246 *Precision* is intended to capture the “completeness” of recall, or how fully the presented content  
247 was recapitulated in a participant’s recounting. We define a recall event’s precision as the maximum  
248 correlation between the topic proportions of that recall event and any episode event (Fig. 4). In  
249 other words, given that a recall event best matches a particular episode event, more precisely  
250 recalled events overlap more strongly with the conceptual content of the original episode event.  
251 When a given event is assigned a blend of several topics, as is often the case (Fig. 2), a high precision  
252 score requires recapitulating the relative topic proportions during recall.

253 *Distinctiveness* is intended to capture the “specificity” of recall. In other words, distinctiveness  
254 quantifies the extent to which a given recall event reflects the most similar episode event over and  
255 above other episode events. Intuitively, distinctiveness is like a normalized variant of our precision  
256 metric. Whereas precision solely measures how much detail about an episode was captured in  
257 someone’s recall, distinctiveness penalizes details that also pertain to other episode events. We  
258 define the distinctiveness of an event’s recall as its precision expressed in standard deviation  
259 units with respect to other episode events. Specifically, for a given recall event, we compute the  
260 correlation between its topic vector and that of each episode event. This yields a distribution of  
261 correlation coefficients (one per episode event). We subtract the mean and divide by the standard  
262 deviation of this distribution to  $z$ -score the coefficients. The maximum value in this distribution  
263 (which, by definition, belongs to the episode event that best matches the given recall event) is that  
264 recall event’s distinctiveness score. In this way, recall events that match one episode event far better  
265 than all other episode events will receive a high distinctiveness score. By contrast, a recall event  
266 that matches all episode events roughly equally will receive a comparatively low distinctiveness  
267 score.

268 In addition to examining how precisely and distinctively participants recalled individual events,  
269 one may also use these metrics to summarize each participant’s performance by averaging across  
270 a participant’s event-wise precision or distinctiveness scores. This enables us to quantify how  
271 precisely a participant tended to recall subtle within-event details, as well as how specific (dis-

tinctive) those details were to individual events from the episode. Participants' average precision and distinctiveness scores were strongly correlated ( $r(15) = 0.90, p < 0.001$ ). This indicates that participants who tended to precisely recount low-level details of episode events also tended to do so in an event-specific way (e.g., as opposed to detailing recurring themes that were present in most or all episode events; this behavior would have resulted in high precision but low distinctiveness). We found that, across participants, higher precision scores were positively correlated with the numbers of both hand-annotated scenes ( $r(15) = 0.60, p = 0.010$ ) and model-estimated events ( $r(15) = 0.90, p < 0.001$ ) that participants recalled. Participants' average distinctiveness scores were also correlated with both the hand-annotated ( $r(15) = 0.45, p = 0.068$ ) and model-estimated ( $r(15) = 0.71, p = 0.001$ ) numbers of recalled events.

Examining individual recalls of the same episode event can provide insights into how the above precision and distinctiveness scores may be used to characterize similarities and differences in how different people describe the same shared experience. In Figure 5, we compare recalls for the same episode event from the participants with the highest (P17) and lowest (P6) precision scores. From the HMM-identified episode event boundaries, we recovered the set of annotations describing the content of a single episode event (event 21; Fig. 5C), and divided them into different color-coded sections for each action or feature described. Next, we used an analogous approach to identify the set of sentences comprising the corresponding recall event from each of the two example participants (Fig. 5D). We then colored all words describing actions and features in the transcripts shown in Panel D according to the color-coded annotations in Panel C. Visual comparison of these example recalls reveals that the more precise recall captures more of the episode event's content, and in greater detail.

Figure 5 also illustrates the differences between high and low distinctiveness scores. We extracted the set of sentences comprising the most distinctive recall event (P9) and least distinctive recall event (P6) corresponding to the example episode event shown in Panel C (event 21). We also extracted the annotations for all episode events whose content these participants' single recall events described. We assigned each episode event a unique color (Fig. 5E), and colored each recalled sentence (Panel F) according to the episode events they best matched. Visual inspection

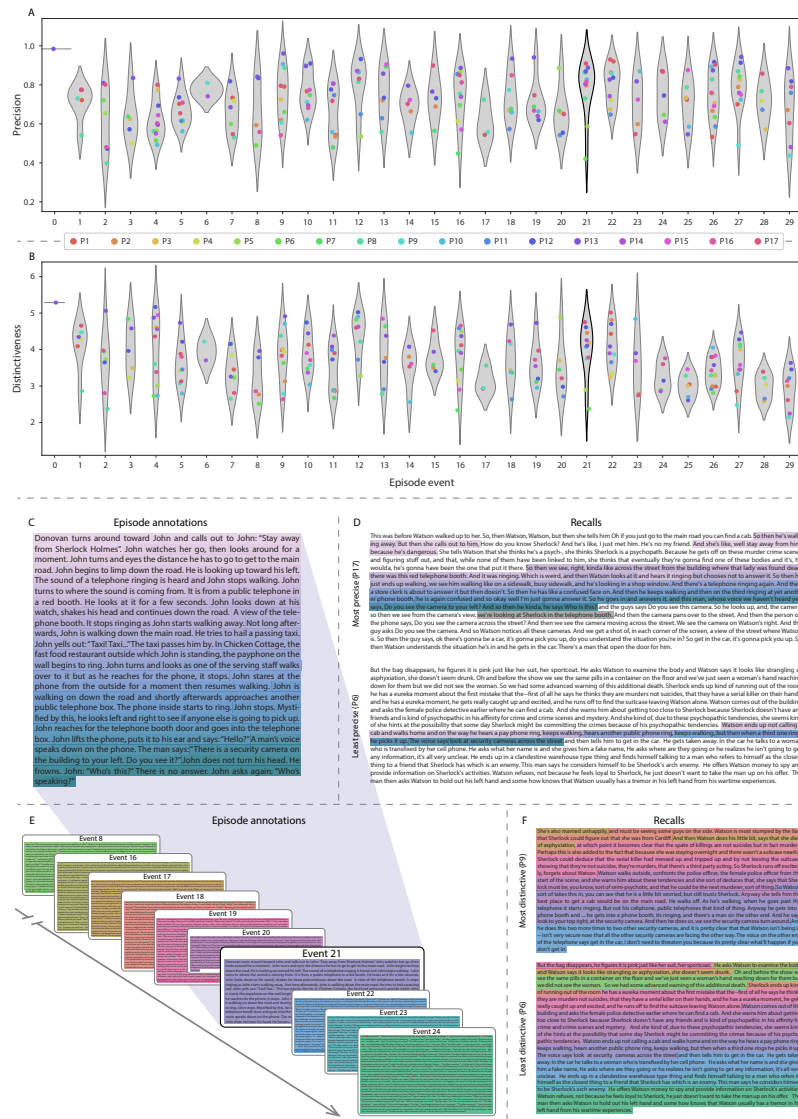


**Figure 5: Precision reflects the completeness of recall, whereas distinctiveness reflects recall specificity.** A. Recall precision by episode event. Grey violin plots display kernel density estimates for the distribution of recall precision scores for a single episode event. Colored dots within each violin plot represent individual participants' recall precision for the given event. B. Recall distinctiveness by episode event, analogous to Panel A. C. The set of "Narrative Details" episode annotations (generated by Chen et al., 2017) comprising an example episode event (22) identified by the HMM. Each action or feature is highlighted in a different color. D. Sentences comprising the most precise (P17) and least precise (P6) participants' recalls of episode event 21. Descriptions of specific actions or features reflecting those highlighted in Panel B are highlighted in the corresponding color. The text highlighted in gray denotes a (rare) false recall. The unhighlighted text denotes correctly recalled information about other episode events. E. The sets of "Narrative Details" episode annotations (generated by Chen et al., 2017) for scenes comprising episode events described by the example participants in Panel F. Each event's text is highlighted in a different color. F. The sentences comprising the most distinctive (P9) and least distinctive (P6) participants' recalls of episode event 21. Sections of recall describing each episode event in Panel E are highlighted with the corresponding color.

300 of Panel F reveals that the most distinctive recall's content is tightly concentrated around event  
301 21, whereas the least distinctive recall incorporates content from a much wider range of episode  
302 events.

303 The preceding analyses sought to characterize how participants' recounts of individual  
304 episode events captured the low-level details of each event. Next, we sought to characterize how  
305 participants' recounts of the full episode captured its high-level essence—i.e., the shape of the  
306 episode's trajectory through word embedding (topic) space. To visualize the essence of the episode  
307 and each participant's recall trajectory (Heusser et al., 2018b), we projected the topic proportions  
308 matrices for the episode and recalls onto a shared two-dimensional space using Uniform Manifold  
309 Approximation and Projection (UMAP; McInnes et al., 2018). In this lower-dimensional space,  
310 each point represents a single episode or recall event, and the distances between the points reflect  
311 the distances between the events' associated topic vectors (Fig. 6). In other words, events that are  
312 nearer to each other in this space are more semantically similar, and those that are farther apart are  
313 less so.

314 Visual inspection of the episode and recall topic trajectories reveals a striking pattern. First,  
315 the topic trajectory of the episode (which reflects its dynamic content; Fig. 6A) is captured nearly  
316 perfectly by the averaged topic trajectories of participants' recalls (Fig. 6B). To assess the consistency  
317 of these recall trajectories across participants, we asked: given that a participant's recall trajectory  
318 had entered a particular location in the reduced topic space, could the position of their *next* recalled  
319 event be predicted reliably? For each location in the reduced topic space, we computed the set of  
320 line segments connecting successively recalled events (across all participants) that intersected that  
321 location (see *Methods*). We then computed (for each location) the distribution of angles formed  
322 by the lines defined by those line segments and a fixed reference line (the *x*-axis). Rayleigh  
323 tests revealed the set of locations in topic space at which these across-participant distributions  
324 exhibited reliable peaks (blue arrows in Fig. 6B reflect significant peaks at  $p < 0.05$ , corrected). We  
325 observed that the locations traversed by nearly the entire episode trajectory exhibited such peaks.  
326 In other words, participants' recalls exhibited similar trajectories to each other that also matched the  
327 trajectory of the original episode (Fig. 6C). This is especially notable when considering the fact that

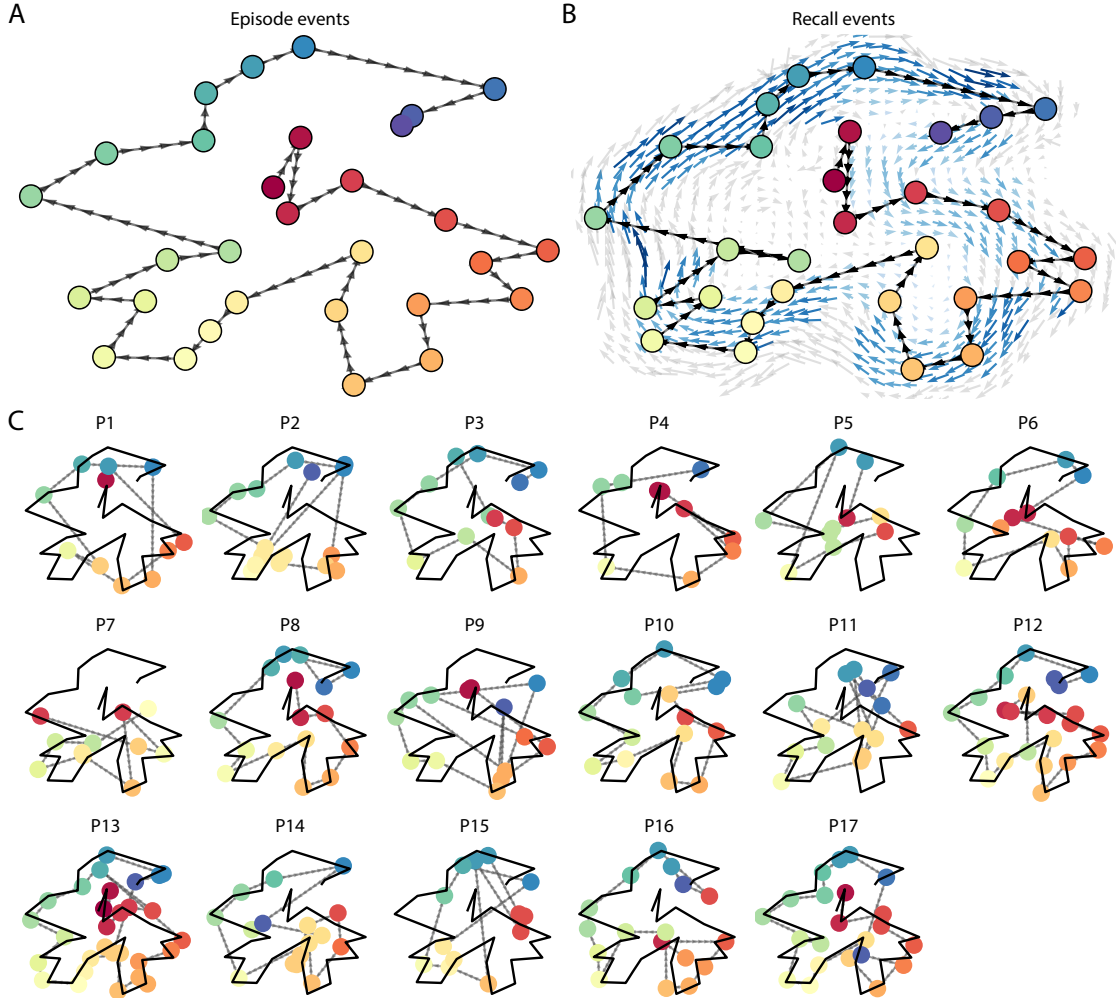


**Figure 6: Trajectories through topic space capture the dynamic content of the episode and recalls.** All panels: the topic proportion matrices have been projected onto a shared two-dimensional space using UMAP. **A.** The two-dimensional topic trajectory taken by the episode of *Sherlock*. Each dot indicates an event identified using the HMM (see *Methods*); the dot colors denote the order of the events (early events are in red; later events are in blue), and the connecting lines indicate the transitions between successive events. **B.** The average two-dimensional trajectory captured by participants' recall sequences, with the same format and coloring as the trajectory in Panel A. To compute the event positions, we matched each recalled event with an event from the original episode (see *Results*), and then we averaged the positions of all events with the same label. The arrows reflect the average transition direction through topic space taken by any participants whose trajectories crossed that part of topic space; blue denotes reliable agreement across participants via a Rayleigh test ( $p < 0.05$ , corrected). **C.** The recall topic trajectories (gray) taken by each individual participant (P1–P17). The episode's trajectory is shown in black for reference. Here, events (dots) are colored by their matched episode event (Panel A).

328 the number of HMM-identified recall events (dots in Fig. 6C) varied considerably across people,  
329 and that every participant used different words to describe what they had remembered happening  
330 in the episode. Differences in the numbers of recall events appear in participants' trajectories  
331 as differences in the sampling resolution along the trajectory. We note that this framework also  
332 provides a means of disentangling classic "proportion recalled" measures (i.e., the proportion of  
333 episode events described in participants' recalls) from participants' abilities to recapitulate the  
334 episode's essence (i.e., the similarity between the shapes of the original episode trajectory and that  
335 defined by each participant's recounting of the episode).

336 In addition to enabling us to visualize the episode's high-level essence, describing the episode  
337 as a geometric trajectory also enables us to drill down to individual words and quantify how each  
338 word relates to the memorability of each event. This provides another approach to examining  
339 participants' recall for low-level details beyond the precision and distinctiveness measures we  
340 defined above. The results displayed in Figures 3C and 5A suggest that certain events were  
341 remembered better than others. Given this, we next asked whether the events that were  
342 generally remembered precisely or imprecisely tended to reflect particular content. Because our  
343 analysis framework projects the dynamic episode content and participants' recalls into a shared  
344 space, and because the dimensions of that space represent topics (which are, in turn, sets of weights  
345 over known words in the vocabulary), we are able to recover the weighted combination of words  
346 that make up any point (i.e., topic vector) in this space. We first computed the average precision  
347 with which participants recalled each of the 30 episode events (Fig. 7A; note that this result is  
348 analogous to a serial position curve created from our precision metric). We then computed a  
349 weighted average of the topic vectors for each episode event, where the weights reflected how  
350 precisely each event was recalled. To visualize the result, we created a "wordle" image (Mueller  
351 et al., 2018) where words weighted more heavily by more precisely-remembered topics appear in  
352 a larger font (Fig. 7B, green box). Across the full episode, content that weighted heavily on topics  
353 and words central to the major foci of the episode (e.g., the names of the two main characters,  
354 "Sherlock" and "John," and the address of a major recurring location, "221B Baker Street") was  
355 best remembered. An analogous analysis revealed which themes were less-precisely remembered.

356 Here in computing the weighted average over events' topic vectors, we weighted each event in  
357 *inverse* proportion to its average precision (Fig. 7B, red box). The least precisely remembered  
358 episode content reflected information that was extraneous to the episode's essence, such as the  
359 proper names of relatively minor characters (e.g., "Mike," "Molly," and "Lestrade") and locations  
360 (e.g., "St. Bartholomew's Hospital").

361 A similar result emerged from assessing the topic vectors for individual episode and recall  
362 events (Fig. 7C). Here, for each of the three most and least precisely remembered episode events, we  
363 have constructed two wordles: one from the original episode event's topic vector (left) and a second  
364 from the average recall topic vector for that event (right). The three most precisely remembered  
365 events (circled in green) correspond to scenes integral to the central plot-line: a mysterious figure  
366 spying on John in a phone booth; John meeting Sherlock at Baker St. to discuss the murders;  
367 and Sherlock laying a trap to catch the killer. Meanwhile, the least precisely remembered events  
368 (circled in red) reflect scenes that comprise minor plot points: a video of singing cartoon characters  
369 that participants viewed in an introductory clip prior to the main episode; John asking Molly  
370 about Sherlock's habit of over-analyzing people; and Sherlock noticing evidence of Anderson's  
371 and Donovan's affair.

372 The results this far inform us about which aspects of the dynamic content in the episode partici-  
373 pants watched were preserved or altered in participants' memories. We next carried out a series of  
374 analyses aimed at understanding which brain structures might facilitate these preservations and  
375 transformations between the participants' shared experience of watching the episode and their  
376 subsequent memories of the episode. In the first analysis, we sought to identify brain structures  
377 that were sensitive to the dynamic unfolding of the episode's content, as characterized by its topic  
378 trajectory. We used a searchlight procedure to identify clusters of voxels whose activity patterns  
379 displayed a proximal temporal correlation structure (as participants watched the episode) match-  
380 ing that of the original episode's topic proportions (Fig. 8A; see *Methods* for additional details). In a  
381 second analysis, we sought to identify brain structures whose responses (during episode viewing)  
382 reflected how each participant would later structure their *recounting* of the episode. We used a  
383 searchlight procedure to identify clusters of voxels whose proximal temporal correlation matrices

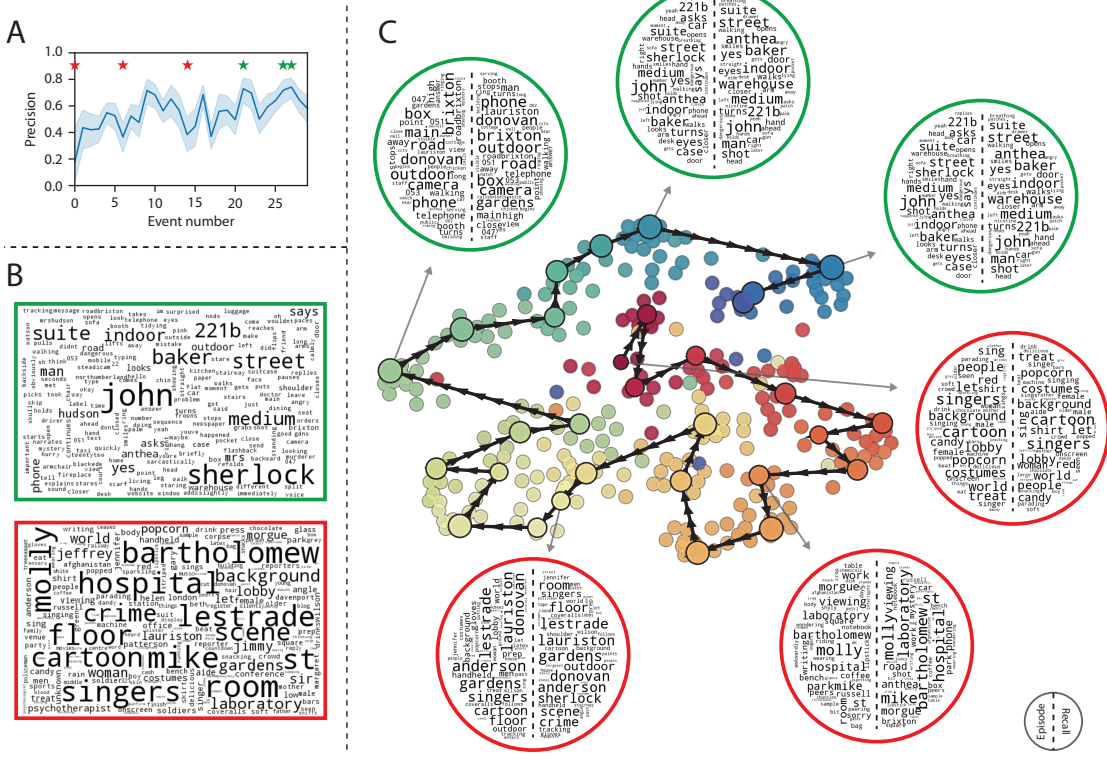


**Figure 7: Language used in the most and least precisely remembered events.** **A.** Average precision (episode event-recall event topic vector correlation) across participants for each episode event. Here we defined each episode event's precision for each participant as the correlation between its topic vector and the most-correlated recall event's topic vector from that participant. Error bars denote bootstrap-derived across-participant 95% confidence intervals. The stars denote the three most precisely remembered events (green) and least precisely remembered events (red). **B.** Wordles comprising the top 200 highest-weighted words reflected in the weighted-average topic vector across episode events. Green: episode events were weighted by their precision (Panel A). Red: episode events were weighted by the inverse of their precision. **C.** The set of all episode and recall events is projected onto the two-dimensional space derived in Figure 6. The dots outlined in black denote episode events (dot size is proportional to each event's average precision). The dots without black outlines denote individual recall events from each participant. All dots are colored using the same scheme as Figure 6A. Wordles for several example events are displayed (green: three most precisely remembered events; red: three least precisely remembered events). Within each circular wordle, the left side displays words associated with the topic vector for the episode event, and the right side displays words associated with the (average) recall event topic vector, across all recall events matched to the given episode event.

384 matched that of the topic proportions matrix for each participant's recall transcript (Figs. 8B; see  
385 *Methods* for additional details). To ensure our searchlight procedure identified regions *specifically*  
386 sensitive to the temporal structure of the episode or recalls (i.e., rather than those with a temporal  
387 autocorrelation length similar to that of the episode and recalls), we performed a phase shift-based  
388 permutation correction (see *Methods*). As shown in Figure 8C, the episode-driven searchlight  
389 analysis revealed a distributed network of regions that may play a role in processing information  
390 relevant to the narrative structure of the episode. The recall-driven searchlight analysis revealed  
391 a second network of regions (Fig. 8D) that may facilitate a person-specific transformation of one's  
392 experience into memory. In identifying regions whose responses to ongoing experiences reflect  
393 how those experiences will be remembered later, this latter analysis extends classic *subsequent*  
394 *memory effect analyses* (e.g., Paller and Wagner, 2002) to the domain of naturalistic experiences.

395 The searchlight analyses described above yielded two distributed networks of brain regions  
396 whose activity timecourses tracked with the temporal structure of the episode (Fig. 8C) or par-  
397 ticipants' subsequent recalls (Fig. 8D). We next sought to gain greater insight into the structures  
398 and functional networks our results reflected. To accomplish this, we performed an additional,  
399 exploratory analysis using Neurosynth (Yarkoni et al., 2011). Given an arbitrary statistical map as  
400 input, Neurosynth performs a massive automated meta-analysis, returning a ranked list of terms  
401 frequently used in neuroimaging papers that report similar statistical maps. We ran Neurosynth  
402 on the (unthresholded) permutation-corrected maps for the episode- and recall-driven searchlight  
403 analyses. The top ten terms with maximally similar meta-analysis images identified by Neurosynth  
404 are shown in Figure 8.

## 405 Discussion

406 Explicitly modeling the dynamic content of a naturalistic stimulus and participants' memories  
407 enabled us to connect the present study of naturalistic recall with an extensive prior literature that  
408 has used list-learning paradigms to study memory (for review see Kahana, 2012), as in Figure 3.  
409 We found some similarities between how participants in the present study recounted a television

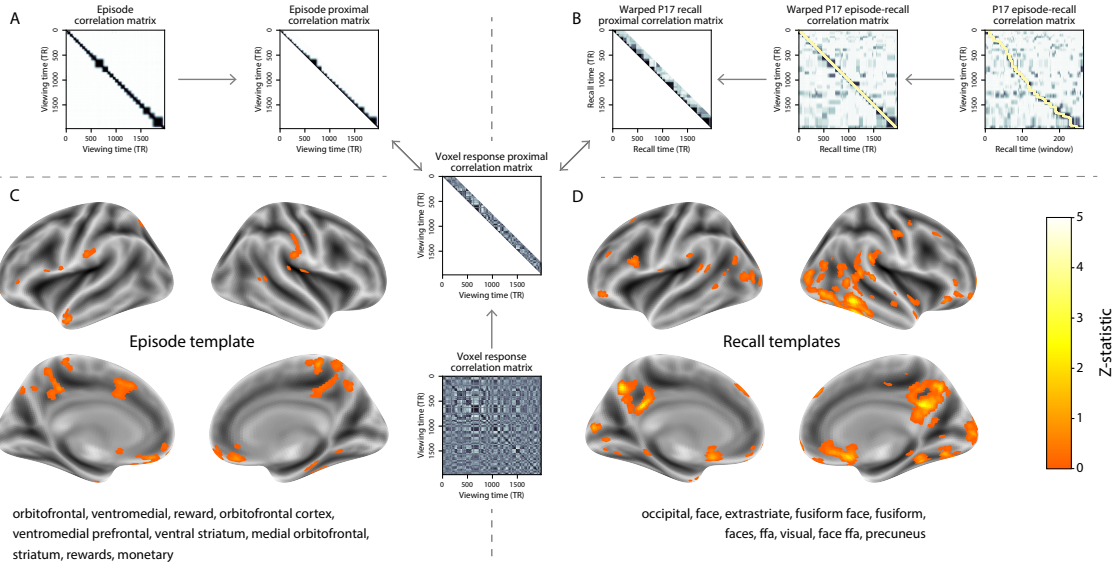


**Figure 8: Brain structures that underlie the transformation of experience into memory.** **A.** We isolated the proximal diagonals from the upper triangle of the episode correlation matrix, and applied this same diagonal mask to the voxel response correlation matrix for each cube of voxels in the brain. We then searched for brain regions whose activation timeseries consistently exhibited a similar proximal correlational structure to the episode model, across participants. **B.** We used dynamic time warping (Berndt and Clifford, 1994) to align each participant’s recall timeseries to the TR timeseries of the episode. We then computed the temporal correlation matrix of each participant’s warped recalls. Next, we applied the same diagonal mask used in Panel A to isolate the proximal temporal correlations and searched for brain regions whose activation timeseries for an individual consistently exhibited a similar proximal correlational structure to each individual’s recalls. **C.** We identified a network of regions sensitive to the narrative structure of participants’ ongoing experience. The map shown is thresholded at  $p < 0.05$ , corrected. The top ten Neurosynth terms displayed in the panel were computed using the unthresholded map. **D.** We also identified a network of regions sensitive to how individuals would later structure the episode’s content in their recalls. The map shown is thresholded at  $p < 0.05$ , corrected. The top ten Neurosynth terms displayed in the panel were computed using the unthresholded map.

410 episode and how participants typically recall memorized random word lists. However, our broader  
411 claim is that word lists miss out on fundamental aspects of naturalistic memory more like the sort  
412 of memory we rely on in everyday life. For example, there are no random word list analogs of  
413 character interactions, conceptual dependencies between temporally distant episode events, the  
414 sense of solving a mystery that pervades the *Sherlock* episode, or the myriad other features of the  
415 episode that convey deep meaning and capture interest. Nevertheless, each of these properties  
416 affects how people process and engage with the episode as they are watching it, and how they  
417 remember it later. The overarching goal of the present study is to characterize how the rich  
418 dynamics of the episode affect the rich behavioral and neural dynamics of how people remember  
419 it.

420 Our work casts remembering as reproducing (behaviorally and neurally) the topic trajectory,  
421 or “shape,” of an experience, thereby drawing implicit analogies between mentally navigating  
422 through word embedding spaces and physically navigating through spatial environments (e.g.,  
423 Bellmund et al., 2020, 2018; Constantinescu et al., 2016). When we characterized memory for  
424 a television episode using this framework, we found that every participant’s recounting of the  
425 episode recapitulated the low spatial frequency details of the shape of its trajectory through topic  
426 space (Fig. 6). We termed this narrative scaffolding the episode’s *essence*. Where participants’  
427 behaviors varied most was in their tendencies to recount specific low-level details from each  
428 episode event. Geometrically, this appears as high spatial frequency distortions in participants’  
429 recall trajectories relative to the trajectory of the original episode (Fig. 7). We developed metrics  
430 to characterize the precision (recovery of any and all event-level information) and distinctiveness  
431 (recovery of event-specific information). We also used word cloud visualizations to interpret the  
432 details of these event-level distortions.

433 The neural analyses we carried out (Fig. 8) also leveraged our geometric framework for char-  
434 acterizing the shapes of the episode and participants’ recounts. We identified one network  
435 of regions whose responses tracked with temporal correlations in the conceptual content of the  
436 episode (as quantified by topic models applied to a set of annotations about the episode). This net-  
437 work included orbitofrontal cortex, ventromedial prefrontal cortex, and striatum, among others.

438 As reviewed by Ranganath and Ritchey (2012), several of these regions are members of the *anterior*  
439 *temporal system*, which has been implicated in assessing and processing the familiarity of ongoing  
440 experiences, emotions, social cognition, and reward. A second network we identified tracked with  
441 temporal correlations in the idiosyncratic conceptual content of participants' subsequent recount-  
442 ings of the episode. This network included occipital cortex, extrastriate cortex, fusiform gyrus, and  
443 the precuneus. Several of these regions are members of the *posterior medial system* (Ranganath and  
444 Ritchey, 2012), which has been implicated in matching incoming cues about the current situation  
445 to internally maintained *situation models* that specify the parameters and expectations inherent to  
446 the current situation (also see Zacks et al., 2007; Zwaan and Radvansky, 1998). Taken together, our  
447 results support the notion that these two (partially overlapping) networks work in coordination  
448 to make sense of our ongoing experiences, distort them in a way that links them with our prior  
449 knowledge and experiences, and encodes those distorted representations into memory for our later  
450 use. Our work also provides a potential framework for modeling and elucidating *memory schemas*—  
451 i.e., cognitive abstractions that may be applied to multiple related experiences (e.g., Baldassano  
452 et al., 2018; Gilboa and Marlatte, 2017). For example, the event-level geometric scaffolding of an  
453 experience (e.g., Fig. 6A) might reflect its underlying schema, and experiences that share similar  
454 schemas might have similar shapes. This could also help explain how brain structures including  
455 the ventromedial prefrontal cortex (Fig. 8; also see Gilboa and Marlatte, 2017) might acquire or  
456 apply schema knowledge across different experiences (i.e., by learning patterns in the schema's  
457 shape).

458 Our general approach draws inspiration from prior work aimed at elucidating the neural and  
459 behavioral underpinnings of how we process dynamic naturalistic experiences and remember them  
460 later. Our approach to identifying neural responses to naturalistic stimuli (including experiences)  
461 entails building an explicit model of the stimulus dynamics and searching for brain regions whose  
462 responses are consistent with the model (also see Huth et al., 2016, 2012). Building an explicit  
463 model of these dynamics also enables us to match up different people's recounts of a common  
464 shared experience, despite individual differences (also see Gagnepain et al., 2020). In prior work,  
465 a series of studies from Uri Hasson's group (Baldassano et al., 2017; Chen et al., 2017; Lerner et al.,

466 2011; Simony et al., 2016; Zadbood et al., 2017) have presented a clever alternative approach: rather  
467 than building an explicit stimulus model, these studies instead search for brain responses to the  
468 stimulus that are reliably similar across individuals. So called *inter-subject correlation* (ISC) and  
469 *inter-subject functional connectivity* (ISFC) analyses effectively treat other people’s brain responses  
470 to the stimulus as a “model” of how its features change over time (also see Simony and Chang,  
471 2020). These purely brain-driven approaches are well suited to identifying which brain structures  
472 exhibit similar stimulus-driven responses across individuals. Further, because neural response  
473 dynamics are observed data (rather than model approximations), such approaches do not require  
474 a detailed understanding of which stimulus properties or features might be driving the observed  
475 responses. However, this also means that the specific stimulus features driving those responses  
476 are typically opaque to the researcher. Our approach is complementary. By explicitly modeling  
477 the stimulus dynamics, we are able to relate specific stimulus features to behavioral and neural  
478 dynamics. However, when our model fails to accurately capture the stimulus dynamics that are  
479 truly driving behavioral and neural responses, our approach necessarily yields an incomplete  
480 characterization of the neural basis of the processes we are studying.

481 Other recent work has used HMMs to discover latent event structure in neural responses  
482 to naturalistic stimuli (Baldassano et al., 2017). By applying HMMs to our explicit models of  
483 stimulus and memory dynamics, we gain a more direct understanding of those state dynamics.  
484 For example, we found that although the events comprising each participant’s recalls recapitulated  
485 the episode’s essence, participants differed in the *resolution* of their recounting of low-level details.  
486 In turn, these individual behavioral differences were reflected in differences in neural activity  
487 dynamics as participants watched the television episode.

488 Our approach also draws inspiration from the growing field of word embedding models. The  
489 topic models (Blei et al., 2003) we used to embed text from the episode annotations and participants’  
490 recall transcripts are just one of many models that have been studied in an extensive literature.  
491 The earliest approaches to word embedding, including latent semantic analysis (Landauer and  
492 Dumais, 1997), used word co-occurrence statistics (i.e., how often pairs of words occur in the  
493 same documents contained in the corpus) to derive a unique feature vector for each word. The

494 feature vectors are constructed so that words that co-occur more frequently have feature vectors  
495 that are closer (in Euclidean distance). Topic models are essentially an extension of those early  
496 models, in that they attempt to explicitly model the underlying causes of word co-occurrences by  
497 automatically identifying the set of themes or topics reflected across the documents in the corpus.  
498 More recent work on these types of semantic models, including word2vec (Mikolov et al., 2013),  
499 the Universal Sentence Encoder (Cer et al., 2018), GPT-2 (Radford et al., 2019), and GTP-3 (Brown  
500 et al., 2020) use deep neural networks to attempt to identify the deeper conceptual representations  
501 underlying each word. Despite the growing popularity of these sophisticated deep learning-based  
502 embedding models, we chose to prioritize interpretability of the embedding dimensions (e.g.,  
503 Fig. 7) over raw performance (e.g., with respect to some predefined benchmark). Nevertheless, we  
504 note that our general framework is, in principle, robust to the specific choice of language model  
505 as well as other aspects of our computational pipeline. For example, the word embedding model,  
506 timeseries segmentation model, and the episode-recall matching function could each be customized  
507 to suit a particular question space or application. Indeed, for some questions, interpretability of  
508 the embeddings may not be a priority, and thus other text embedding approaches (including the  
509 deep learning-based models described above) may be preferable. Further work will be needed to  
510 explore the influence of particular models on our framework’s predictions and performance.

511 Our work has broad implications for how we characterize and assess memory in real-world  
512 settings, such as the classroom or physician’s office. For example, the most commonly used  
513 classroom evaluation tools involve simply computing the proportion of correctly answered exam  
514 questions. Our work indicates that this approach is only loosely related to what educators might  
515 really want to measure: how well did the students understand the key ideas presented in the  
516 course? Under this typical framework of assessment, the same exam score of 50% could be ascribed  
517 to two very different students: one who attended to the full course but struggled to learn more than  
518 a broad overview of the material, and one who attended to only half of the course but understood  
519 the attended material perfectly. Instead, one could apply our computational framework to build  
520 explicit dynamic content models of the course material and exam questions. This approach would  
521 provide a more nuanced and specific view into which aspects of the material students had learned

522 well (or poorly). In clinical settings, memory measures that incorporate such explicit content  
523 models might also provide more direct evaluations of patients' memories, and of doctor-patient  
524 interactions.

## 525 Methods

### 526 Paradigm and data collection

527 Data were collected by Chen et al. (2017). In brief, participants ( $n = 22$ ) viewed the first 48 minutes  
528 of "A Study in Pink," the first episode of the BBC television show *Sherlock*, while fMRI volumes  
529 were collected (TR = 1500 ms). Participants were pre-screened to ensure they had never seen any  
530 episode of the show before. The stimulus was divided into a 23 min (946 TR) and a 25 min (1030 TR)  
531 segment to mitigate technical issues related to the scanner. After finishing the clip, participants  
532 were instructed to (quoting from Chen et al., 2017) "describe what they recalled of the [episode]  
533 in as much detail as they could, to try to recount events in the original order they were viewed  
534 in, and to speak for at least 10 minutes if possible but that longer was better. They were told that  
535 completeness and detail were more important than temporal order, and that if at any point they  
536 realized they had missed something, to return to it. Participants were then allowed to speak for  
537 as long as they wished, and verbally indicated when they were finished (e.g., 'I'm done')." Five  
538 participants were dropped from the original dataset due to excessive head motion (2 participants),  
539 insufficient recall length (2 participants), or falling asleep during stimulus viewing (1 participant),  
540 resulting in a final sample size of  $n = 17$ . For additional details about the testing procedures  
541 and scanning parameters, see Chen et al. (2017). The testing protocol was approved by Princeton  
542 University's Institutional Review Board.

543 After preprocessing the fMRI data and warping the images into a standard (3 mm<sup>3</sup> MNI) space,  
544 the voxel activations were z-scored (within voxel) and spatially smoothed using a 6 mm (full width  
545 at half maximum) Gaussian kernel. The fMRI data were also cropped so that all episode-viewing  
546 data were aligned across participants. This included a constant 3 TR (4.5 s) shift to account for the

547 lag in the hemodynamic response. (All of these preprocessing steps followed Chen et al., 2017,  
548 where additional details may be found.)

549 The video stimulus was divided into 1,000 fine-grained “time segments” and annotated by an  
550 independent coder. For each of these 1,000 annotations, the following information was recorded:  
551 a brief narrative description of what was happening, the location where the time segment took  
552 place, whether that location was indoors or outdoors, the names of all characters on-screen, the  
553 name(s) of the character(s) in focus in the shot, the name(s) of the character(s) currently speaking,  
554 the camera angle of the shot, a transcription of any text appearing on-screen, and whether or not  
555 there was music present in the background. Each time segment was also tagged with its onset and  
556 offset time, in both seconds and TRs.

## 557 **Data and code availability**

558 The fMRI data we analyzed are available online [here](#). The behavioral data and all of our analysis  
559 code may be downloaded [here](#).

## 560 **Statistics**

561 All statistical tests performed in the behavioral analyses were two-sided. All statistical tests per-  
562 formed in the neural data analyses were two-sided, except for the permutation-based thresholding,  
563 which was one-sided. In this case, we were specifically interested in identifying voxels whose ac-  
564 tivation time series reflected the temporal structure of the episode and recall topic proportions  
565 matrices to a *greater* extent than that of the phase-shifted matrices.

## 566 **Modeling the dynamic content of the episode and recall transcripts**

### 567 **Topic modeling**

568 The input to the topic model we trained to characterize the dynamic content of the episode  
569 comprised 998 hand-generated annotations of short (mean: 2.96s) time segments spanning the  
570 video clip (Chen et al., 2017 generated 1000 annotations total; we removed two annotations referring

571 to a break between the first and second scan sessions, during which no fMRI data were collected).  
572 We concatenated the text for all of the annotated features within each segment, creating a “bag of  
573 words” describing its content and performed some minor preprocessing (e.g., stemming possessive  
574 nouns and removing punctuation). We then re-organized the text descriptions into overlapping  
575 sliding windows spanning (up to) 50 annotations each. In other words, we estimated the “context”  
576 for each annotated segment using the text descriptions of the preceding 25 annotations, the present  
577 annotations, and the following 24 annotations. To model the context for annotations near the  
578 beginning of the episode (i.e., within 25 of the beginning or end), we created overlapping sliding  
579 windows that grew in size from one annotation to the full length. We also tapered the sliding  
580 window lengths at the end of the episode, whereby time segments within fewer than 24 annotations  
581 of the end of the episode were assigned sliding windows that extended to the end of the episode.  
582 This procedure ensured that each annotation’s content was represented in the text corpus an equal  
583 number of times.

584 We trained our model using these overlapping text samples with `scikit-learn` (version 0.19.1;  
585 Pedregosa et al., 2011), called from our high-dimensional visualization and text analysis software,  
586 `HyperTools` (Heusser et al., 2018b). Specifically, we used the `CountVectorizer` class to transform  
587 the text from each window into a vector of word counts (using the union of all words across  
588 all annotations as the “vocabulary,” excluding English stop words); this yielded a number-of-  
589 windows by number-of-words *word count* matrix. We then used the `LatentDirichletAllocation`  
590 class (`topics=100, method='batch'`) to fit a topic model (Blei et al., 2003) to the word count matrix,  
591 yielding a number-of-windows (1047) by number-of-topics (100) *topic proportions* matrix. The  
592 topic proportions matrix describes the gradually evolving mix of topics (latent themes) present  
593 in each annotated time segment of the episode. Next, we transformed the topic proportions  
594 matrix to match the 1976 fMRI volume acquisition times. We assigned each topic vector to the  
595 timepoint (in seconds) midway between the beginning of the first annotation and the end of the last  
596 annotation in its corresponding sliding text window. By doing so, we warped the linear temporal  
597 distance between consecutive topic vectors to align with the inconsistent temporal distance between  
598 consecutive annotations (whose durations varied greatly). We then rescaled these timepoints to

599 1.5s TR units, and used linear interpolation to estimate a topic vector for each TR. This resulted in  
600 a number-of-TRs (1976) by number-of-topics (100) matrix.

601 We created similar topic proportions matrices using hand-annotated transcripts of each partic-  
602 ipant’s verbal recall of the episode (annotated by Chen et al., 2017). We tokenized the transcript  
603 into a list of sentences, and then re-organized the list into overlapping sliding windows spanning  
604 (up to) 10 sentences each, analogously to how we parsed the episode annotations. In turn, we  
605 transformed each window’s sentences into a word count vector (using the same vocabulary as for  
606 the episode model), then used the topic model already trained on the episode scenes to compute  
607 the most probable topic proportions for each sliding window. This yielded a number-of-windows  
608 (range: 83–312) by number-of-topics (100) topic proportions matrix for each participant. These  
609 reflected the dynamic content of each participant’s recalls. Note: for details on how we selected the  
610 episode and recall window lengths and number of topics, see *Supporting Information* and Figure S1.

611 **Segmenting topic proportions matrices into discrete events using hidden Markov Models**

612 We parsed the topic proportions matrices of the episode and participants’ recalls into discrete  
613 events using hidden Markov Models (HMMs; Rabiner, 1989). Given the topic proportions matrix  
614 (describing the mix of topics at each timepoint) and a number of states,  $K$ , an HMM recovers the  
615 set of state transitions that segments the timeseries into  $K$  discrete states. Following Baldassano  
616 et al. (2017), we imposed an additional set of constraints on the discovered state transitions that  
617 ensured that each state was encountered exactly once (i.e., never repeated). We used the BrainIAK  
618 toolbox (Capota et al., 2017) to implement this segmentation.

619 We used an optimization procedure to select the appropriate  $K$  for each topic proportions  
620 matrix. Prior studies on narrative structure and processing have shown that we both perceive  
621 and internally represent the world around us at multiple, hierarchical timescales (e.g., Baldassano  
622 et al., 2017, 2018; Chen et al., 2017; Hasson et al., 2015, 2008; Lerner et al., 2011). However, for the  
623 purposes of our framework, we sought to identify the single timeseries of event-representations  
624 that is emphasized *most heavily* in the temporal structure of the episode and of each participant’s  
recall. We quantified this as the set of  $K$  states that maximized the similarity between topic vectors

for timepoints comprising each state, while minimizing the similarity between topic vectors for timepoints across different states. Specifically, we computed (for each matrix)

$$\operatorname{argmax}_K [W_1(a, b)],$$

where  $a$  was the distribution of within-state topic vector correlations, and  $b$  was the distribution of across-state topic vector correlations. We computed the first Wasserstein distance ( $W_1$ ; also known as *Earth mover's distance*; Dobrushin, 1970; Ramdas et al., 2017) between these distributions for a large range of possible  $K$ -values (range [2, 50]), and selected the  $K$  that yielded the maximum value. Figure 2B displays the event boundaries returned for the episode, and Figure S4 displays the event boundaries returned for each participant's recalls. See Figure S6 for the optimization functions for the episode and recalls. After obtaining these event boundaries, we created stable estimates of the content represented in each event by averaging the topic vectors across timepoints between each pair of event boundaries. This yielded a number-of-events by number-of-topics matrix for the episode and recalls from each participant.

### 638 Naturalistic extensions of classic list-learning analyses

In traditional list-learning experiments, participants view a list of items (e.g., words) and then recall the items later. Our episode-recall event matching approach affords us the ability to analyze memory in a similar way. The episode and recall events can be treated analogously to studied and recalled "items" in a list-learning study. We can then extend classic analyses of memory performance and dynamics (originally designed for list-learning experiments) to the more naturalistic episode recall task used in this study.

Perhaps the simplest and most widely used measure of memory performance is *accuracy*—i.e., the proportion of studied (experienced) items (in this case, episode events) that the participant later remembered. Chen et al. (2017) used this method to rate each participant's memory quality by computing the proportion of (50, manually identified) scenes mentioned in their recall. We found a strong across-participants correlation between these independent ratings and the proportion of 30

650 HMM-identified episode events matched to participants' recalls (Pearson's  $r(15) = 0.71, p = 0.002$ ).  
651 We further considered a number of more nuanced memory performance measures that are typically  
652 associated with list-learning studies. We also provide a software package, Quail, for carrying out  
653 these analyses (Heusser et al., 2017).

654 **Probability of first recall (PFR).** PFR curves (Atkinson and Shiffrin, 1968; Postman and Phillips,  
655 1965; Welch and Burnett, 1924) reflect the probability that an item will be recalled first, as a  
656 function of its serial position during encoding. To carry out this analysis, we initialized a number-  
657 of-participants (17) by number-of-episode-events (30) matrix of zeros. Then, for each participant,  
658 we found the index of the episode event that was recalled first (i.e., the episode event whose topic  
659 vector was most strongly correlated with that of the first recall event) and filled in that index in  
660 the matrix with a 1. Finally, we averaged over the rows of the matrix, resulting in a 1 by 30 array  
661 representing the proportion of participants that recalled an event first, as a function of the order of  
662 the event's appearance in the episode (Fig. 3A).

663 **Lag conditional probability curve (lag-CRP).** The lag-CRP curve (Kahana, 1996) reflects the  
664 probability of recalling a given item after the just-recalled item, as a function of their relative  
665 encoding positions (or *lag*). In other words, a lag of 1 indicates that a recalled item was presented  
666 immediately after the previously recalled item, and a lag of -3 indicates that a recalled item came 3  
667 items before the previously recalled item. For each recall transition (following the first recall), we  
668 computed the lag between the current recall event and the next recall event, normalizing by the  
669 total number of possible transitions. This yielded a number-of-participants (17) by number-of-lags  
670 (-29 to +29; 58 lags total excluding lags of 0) matrix. We averaged over the rows of this matrix to  
671 obtain a group-averaged lag-CRP curve (Fig. 3B).

672 **Serial position curve (SPC).** SPCs (Murdock, 1962) reflect the proportion of participants that  
673 remember each item as a function of the item's serial position during encoding. We initialized  
674 a number-of-participants (17) by number-of-episode-events (30) matrix of zeros. Then, for each  
675 recalled event, for each participant, we found the index of the episode event that the recalled

676 event most closely matched (via the correlation between the events' topic vectors) and entered a  
677 1 into that position in the matrix. This resulted in a matrix whose entries indicated whether or  
678 not each event was recalled by each participant (depending on whether the corresponding entires  
679 were set to one or zero). Finally, we averaged over the rows of the matrix to yield a 1 by 30 array  
680 representing the proportion of participants that recalled each event as a function of the events'  
681 order appearance in the episode (Fig. 3C).

682 **Temporal clustering scores.** Temporal clustering describes a participant's tendency to organize  
683 their recall sequences by the learned items' encoding positions. For instance, if a participant  
684 recalled the episode events in the exact order they occurred (or in exact reverse order), this would  
685 yield a score of 1. If a participant recalled the events in random order, this would yield an expected  
686 score of 0.5. For each recall event transition (and separately for each participant), we sorted all  
687 not-yet-recalled events according to their absolute lag (i.e., distance away in the episode). We  
688 then computed the percentile rank of the next event the participant recalled. We averaged these  
689 percentile ranks across all of the participant's recalls to obtain a single temporal clustering score  
690 for the participant.

691 **Semantic clustering scores.** Semantic clustering describes a participant's tendency to recall se-  
692 mantically similar presented items together in their recall sequences. Here, we used the topic  
693 vectors for each event as a proxy for its semantic content. Thus, the similarity between the seman-  
694 tic content for two events can be computed by correlating their respective topic vectors. For each  
695 recall event transition, we sorted all not-yet-recalled events according to how correlated the topic  
696 vector of the closest-matching episode event was to the topic vector of the closest-matching episode  
697 event to the just-recalled event. We then computed the percentile rank of the observed next recall.  
698 We averaged these percentile ranks across all of the participant's recalls to obtain a single semantic  
699 clustering score for the participant.

700 **Averaging correlations**

701 In all instances where we performed statistical tests involving precision or distinctiveness scores  
702 (Fig. 5), we used the Fisher  $z$ -transformation (Fisher, 1925) to stabilize the variance across the  
703 distribution of correlation values prior to performing the test. Similarly, when averaging precision  
704 or distinctiveness scores, we  $z$ -transformed the scores prior to computing the mean, and inverse  
705  $z$ -transformed the result.

706 **Visualizing the episode and recall topic trajectories**

707 We used the UMAP algorithm (McInnes et al., 2018) to project the 100-dimensional topic space onto  
708 a two-dimensional space for visualization (Figs. 6, 7). To ensure that all of the trajectories were  
709 projected onto the *same* lower dimensional space, we computed the low-dimensional embedding  
710 on a “stacked” matrix created by vertically concatenating the events-by-topics topic proportions  
711 matrices for the episode, across-participants average recall and all 17 individual participants’ re-  
712 calls. We then separated the rows of the result (a total-number-of-events by two matrix) back into  
713 individual matrices for the episode topic trajectory, across-participant average recall trajectory,  
714 and the trajectories for each individual participant’s recalls (Fig. 6). This general approach for dis-  
715 covering a shared low-dimensional embedding for a collections of high-dimensional observations  
716 follows Heusser et al. (2018b).

717 We optimized the manifold space for visualization based on two criteria: First, that the 2D em-  
718 bedding of the episode trajectory should reflect its original 100-dimensional structure as faithfully  
719 as possible. Second, that the path traversed by the embedded episode trajectory should intersect  
720 itself a minimal number of times. The first criteria helps bolster the validity of visual intuitions  
721 about relationships between sections of episode content, based on their locations in the embed-  
722 ding space. The second criteria was motivated by the observed low off-diagonal values in the  
723 episode trajectory’s temporal correlation matrix (suggesting that the same topic-space coordinates  
724 should not be revisited; see Fig. 2A). For further details on how we created this low-dimensional  
725 embedding space, see *Supporting Information*.

726 **Estimating the consistency of flow through topic space across participants**

727 In Figure 6B, we present an analysis aimed at characterizing locations in topic space that dif-  
728 ferent participants move through in a consistent way (via their recall topic trajectories). The  
729 two-dimensional topic space used in our visualizations (Fig. 6) comprised a  $60 \times 60$  (arbitrary  
730 units) square. We tiled this space with a  $50 \times 50$  grid of evenly spaced vertices, and defined a  
731 circular area centered on each vertex whose radius was two times the distance between adjacent  
732 vertices (i.e., 2.4 units). For each vertex, we examined the set of line segments formed by connecting  
733 each pair successively recalled events, across all participants, that passed through this circle. We  
734 computed the distribution of angles formed by those segments and the  $x$ -axis, and used a Rayleigh  
735 test to determine whether the distribution of angles was reliably “peaked” (i.e., consistent across  
736 all transitions that passed through that local portion of topic space). To create Figure 6B, we drew  
737 an arrow originating from each grid vertex, pointing in the direction of the average angle formed  
738 by the line segments that passed within 2.4 units. We set the arrow lengths to be inversely propor-  
739 tional to the  $p$ -values of the Rayleigh tests at each vertex. Specifically, for each vertex we converted  
740 all of the angles of segments that passed within 2.4 units to unit vectors, and we set the arrow  
741 lengths at each vertex proportional to the length of the (circular) mean vector. We also indicated  
742 any significant results ( $p < 0.05$ , corrected using the Benjamani-Hochberg procedure) by coloring  
743 the arrows in blue (darker blue denotes a lower  $p$ -value, i.e., a longer mean vector); all tests with  
744  $p \geq 0.05$  are displayed in gray and given a lower opacity value.

745 **Searchlight fMRI analyses**

746 In Figure 8, we present two analyses aimed at identifying brain regions whose responses (as partic-  
747 ipants viewed the episode) exhibited a particular temporal structure. We developed a searchlight  
748 analysis wherein we constructed a  $5 \times 5 \times 5$  cube of voxels (following Chen et al., 2017) centered  
749 on each voxel in the brain, and for each of these cubes, computed the temporal correlation matrix  
750 of the voxel responses during episode viewing. Specifically, for each of the 1976 volumes collected  
751 during episode viewing, we correlated the activity patterns in the given cube with the activity

752 patterns (in the same cube) collected during every other timepoint. This yielded a  $1976 \times 1976$   
753 correlation matrix for each cube. Note: participant 5's scan ended 75s early, and in Chen et al.  
754 (2017)'s publicly released dataset, their scan data was zero-padded to match the length of the other  
755 participants'. For our searchlight analyses, we removed this padded data (i.e., the last 50 TRs),  
756 resulting in a  $1925 \times 1925$  correlation matrix for each cube in participant 5's brain.

757 Next, we constructed a series of "template" matrices. The first template reflected the time-  
758 course of the episode's topic proportions matrix, and the others reflected the timecourse of each  
759 participant's recall topic proportions matrix. To construct the episode template, we computed the  
760 correlations between the topic proportions estimated for every pair of TRs (prior to segmenting  
761 the topic proportions matrices into discrete events; i.e., the correlation matrix shown in Figs. 2B  
762 and 8A). We constructed similar temporal correlation matrices for each participant's recall topic  
763 proportions matrix (Figs. 2D, S4). However, to correct for length differences and potential non-  
764 linear transformations between viewing time and recall time, we first used dynamic time warping  
765 (Berndt and Clifford, 1994) to temporally align participants' recall topic proportions matrices  
766 with the episode topic proportions matrix. An example correlation matrix before and after warping  
767 is shown in Fig. 8B. This yielded a  $1976 \times 1976$  correlation matrix for the episode template and for  
768 each participant's recall template.

769 The temporal structure of the episode's content (as described by our model) is captured in the  
770 block-diagonal structure of the episode's temporal correlation matrix (e.g., Figs. 2B, 8A), with time  
771 periods of thematic stability represented as dark blocks of varying sizes. Inspecting the episode  
772 correlation matrix suggests that the episode's semantic content is highly temporally specific (i.e., the  
773 correlations between topic vectors from distant timepoints are almost all near zero). By contrast,  
774 the activity patterns of individual (cubes of) voxels can encode relatively limited information  
775 on their own, and their activity frequently contributes to multiple separate functions (Charron  
776 and Koechlin, 2010; Freedman et al., 2001; Rishel et al., 2013; Sigman and Dehaene, 2008). By  
777 nature, these two attributes give rise to similarities in activity across large timescales that may not  
778 necessarily reflect a single task. To enable a more sensitive analysis of brain regions whose shifts  
779 in activity patterns mirrored shifts in the semantic content of the episode or recalls, we restricted

780 the temporal correlations we considered to the timescale of semantic information captured by our  
781 model. Specifically, we isolated the upper triangle of the episode correlation matrix and created a  
782 “proximal correlation mask” that included only diagonals from the upper triangle of the episode  
783 correlation matrix up to the first diagonal that contained no positive correlations. Applying this  
784 mask to the full episode correlation matrix was equivalent to excluding diagonals beyond the  
785 corner of the largest diagonal block. In other words, the timescale of temporal correlations we  
786 considered corresponded to the longest period of thematic stability in the episode, and by extension  
787 the longest period of thematic stability in participants’ recalls and the longest period of stability we  
788 might expect to see in voxel activity arising from processing or encoding episode content. Figure 8  
789 shows this proximal correlation mask applied to the temporal correlation matrices for the episode,  
790 an example participant’s (warped) recall, and an example cube of voxels from our searchlight  
791 analyses.

792 To determine which (cubes of) voxel responses matched the episode template, we correlated  
793 the proximal diagonals from the upper triangle of the voxel correlation matrix for each cube with  
794 the proximal diagonals from episode template matrix (Kriegeskorte et al., 2008). This yielded, for  
795 each participant, a voxelwise map of correlation values. We then performed a one-sample  $t$ -test  
796 on the distribution of (Fisher  $z$ -transformed) correlations at each voxel, across participants. This  
797 resulted in a value for each voxel (cube), describing how reliably its timecourse followed that of  
798 the episode.

799 We further sought to ensure that our analysis identified regions where the activations’ temporal  
800 structure specifically reflected that of the episode, rather than regions whose activity was simply  
801 autocorrelated at a timescale similar to the episode template’s diagonal. To achieve this, we used  
802 a phase shift-based permutation procedure, whereby we circularly shifted the episode’s topic  
803 proportions matrix by a random number of timepoints (rows), computed the resulting “null”  
804 episode template, and re-ran the searchlight analysis, in full. (For each of the 100 permutations, the  
805 same random shift was used for all participants). We  $z$ -scored the observed (unshifted) result at  
806 each voxel against the distribution of permutation-derived “null” results, and estimated a  $p$ -value  
807 by computing the proportion of shifted results that yielded larger values. To create the map in

808 Figure 8C, we thresholded out any voxels whose similarity to the unshifted episode's structure fell  
809 below the 95<sup>th</sup> percentile of the permutation-derived similarity results.

810 We used an analogous procedure to identify which voxels' responses reflected the recall tem-  
811 plates. For each participant, we correlated the proximal diagonals from the upper triangle of the  
812 correlation matrix for each cube of voxels with the proximal diagonals from the upper triangle  
813 of their (time-warped) recall correlation matrix. As in the episode template analysis, this yielded  
814 a voxelwise map of correlation coefficients for each participant. However, whereas the episode  
815 analysis compared every participant's responses to the same template, here the recall templates  
816 were unique for each participant. As in the analysis described above, we *t*-scored the (Fisher *z*-  
817 transformed) voxelwise correlations, and used the same permutation procedure we developed for  
818 the episode responses to ensure specificity to the recall timeseries and assign significance values.  
819 To create the map in Figure 8D we again thresholded out any voxels whose scores were below the  
820 95<sup>th</sup> percentile of the permutation-derived null distribution.

## 821 **Neurosynth decoding analyses**

822 Neurosynth parses a massive online database of over 14,000 neuroimaging studies and constructs  
823 meta-analysis images for over 13,000 psychology- and neuroscience-related terms, based on NIfTI  
824 images accompanying studies where those terms appear at a high frequency. Given a novel image  
825 (tagged with its value type; e.g., *z*-, *t*-, *F*- or *p*-statistics), Neurosynth returns a list of terms whose  
826 meta-analysis images are most similar. Our permutation procedure yielded, for each of the two  
827 searchlight analyses, a voxelwise map of *z*-values. These maps describe the extent to which each  
828 voxel *specifically* reflected the temporal structure of the episode or individuals' recalls (i.e., relative  
829 to the null distributions of phase-shifted values). We inputted the two statistical maps described  
830 above to Neurosynth to create a list of the 10 most representative terms for each map.

831 **References**

- 832 Atkinson, R. C. and Shiffrin, R. M. (1968). Human memory: A proposed system and its control  
833 processes. In Spence, K. W. and Spence, J. T., editors, *The psychology of learning and motivation*,  
834 volume 2, pages 89–105. Academic Press, New York.
- 835 Baldassano, C., Chen, J., Zadbood, A., Pillow, J. W., Hasson, U., and Norman, K. A. (2017).  
836 Discovering event structure in continuous narrative perception and memory. *Neuron*, 95(3):709–  
837 721.
- 838 Baldassano, C., Hasson, U., and Norman, K. A. (2018). Representation of real-world event schemas  
839 during narrative perception. *Journal of Neuroscience*, 38(45):9689–9699.
- 840 Bellmund, J. L. S., de Cothi, W., Ruiter, T. A., Nau, M., Barry, C., and Doeller, C. F. (2020). Deforming  
841 the metric of cognitive maps distorts memory. *Nature Human Behavior*, 4:177–188.
- 842 Bellmund, J. L. S., Gärdenfors, P., Moser, E. I., and Doeller, C. F. (2018). Navigating cognition:  
843 spatial codes for human thinking. *Science*, 362(6415).
- 844 Berndt, D. J. and Clifford, J. (1994). Using dynamic time warping to find patterns in time series. In  
845 *KDD workshop*, volume 10, pages 359–370.
- 846 Blei, D. M. and Lafferty, J. D. (2006). Dynamic topic models. In *Proceedings of the 23rd International*  
847 *Conference on Machine Learning*, ICML ’06, pages 113–120, New York, NY, US. ACM.
- 848 Blei, D. M., Ng, A. Y., and Jordan, M. I. (2003). Latent dirichlet allocation. *Journal of Machine*  
849 *Learning Research*, 3:993 – 1022.
- 850 Brown, T. B., Mann, B., Ryder, N., Subbiah, M., Kaplan, J., Dhariwal, P., Neelakantan, A., Shyam,  
851 P., Sastry, G., Askell, A., Agarwal, S., Herbert-Voss, A., Krueger, G., Henighan, T., Child, R.,  
852 Ramesh, A., Ziegler, D. M., Wu, J., Winter, C., Hesse, C., Chen, M., Sigler, E., Litwin, M., Gray, S.,  
853 Chess, B., Clark, J., Berner, C., McCandlish, S., Radford, A., Sutskever, I., and Amodei, D. (2020).  
854 Language models are few-shot learners. *arXiv*, 2005.14165.

- 855 Brunec, I. K., Moscovitch, M. M., and Barense, M. D. (2018). Boundaries shape cognitive representations of spaces and events. *Trends in Cognitive Sciences*, 22(7):637–650.
- 856
- 857 Capota, M., Turek, J., Chen, P.-H., Zhu, X., Manning, J. R., Sundaram, N., Keller, B., Wang, Y., and  
858 Shin, Y. S. (2017). Brain imaging analysis kit.
- 859 Cer, D., Yang, Y., Kong, S. Y., Hua, N., Limtiaco, N., John, R. S., Constant, N., Guajardo-Cespedes,  
860 M., Yuan, S., Tar, C., Sung, Y.-H., Strope, B., and Kurzweil, R. (2018). Universal sentence encoder.  
861 *arXiv*, 1803.11175.
- 862 Charron, S. and Koechlin, E. (2010). Divided representations of current goals in the human frontal  
863 lobes. *Science*, 328(5976):360–363.
- 864 Chen, J., Leong, Y. C., Honey, C. J., Yong, C. H., Norman, K. A., and Hasson, U. (2017). Shared  
865 memories reveal shared structure in neural activity across individuals. *Nature Neuroscience*,  
866 20(1):115.
- 867 Clewett, D. and Davachi, L. (2017). The ebb and flow of experience determines the temporal  
868 structure of memory. *Curr Opin Behav Sci*, 17:186–193.
- 869 Constantinescu, A. O., O'Reilly, J. X., and Behrens, T. E. J. (2016). Organizing conceptual knowledge  
870 in humans with a gridlike code. *Science*, 352(6292):1464–1468.
- 871 Dobrushin, R. L. (1970). Prescribing a system of random variables by conditional distributions.  
872 *Theory of Probability & Its Applications*, 15(3):458–486.
- 873 DuBrow, S. and Davachi, L. (2013). The influence of contextual boundaries on memory for the  
874 sequential order of events. *Journal of Experimental Psychology: General*, 142(4):1277–1286.
- 875 Ezzyat, Y. and Davachi, L. (2011). What constitutes an episode in episodic memory? *Psychological  
876 Science*, 22(2):243–252.
- 877 Fisher, R. A. (1925). *Statistical Methods for Research Workers*. Oliver and Boyd.

- 878 Freedman, D., Riesenhuber, M., Poggio, T., and Miller, E. (2001). Categorical representation of  
879 visual stimuli in the primate prefrontal cortex. *Science*, 291(5502):312–316.
- 880 Gagnepain, P., Vallée, T., Heiden, S., Decorde, M., Gauvain, J.-L., Laurent, A., Klein-Peschanski, C.,  
881 Viader, F., Peschanski, D., and Eustache, F. (2020). Collective memory shapes the organization  
882 of individual memories in the medial prefrontal cortex. *Nature Human Behavior*, 4:189–200.
- 883 Gilboa, A. and Marlatte, H. (2017). Neurobiology of schemas and schema-mediated memory.  
884 *Trends Cogn Sci*, 21(8):618–631.
- 885 Hasson, U., Chen, J., and Honey, C. J. (2015). Hierarchical process memory: memory as an integral  
886 component of information processing. *Trends in Cognitive Science*, 19(6):304–315.
- 887 Hasson, U., Yang, E., Vallines, I., Heeger, D. J., and Rubin, N. (2008). A hierarchy of temporal  
888 receptive windows in human cortex. *Journal of Neuroscience*, 28(10):2539–2550.
- 889 Heusser, A. C., Ezzyat, Y., Shiff, I., and Davachi, L. (2018a). Perceptual boundaries cause mnemonic  
890 trade-offs between local boundary processing and across-trial associative binding. *Journal of*  
891 *Experimental Psychology Learning, Memory, and Cognition*, 44(7):1075–1090.
- 892 Heusser, A. C., Fitzpatrick, P. C., Field, C. E., Ziman, K., and Manning, J. R. (2017). Quail: a  
893 Python toolbox for analyzing and plotting free recall data. *The Journal of Open Source Software*,  
894 10.21105/joss.00424.
- 895 Heusser, A. C., Ziman, K., Owen, L. L. W., and Manning, J. R. (2018b). HyperTools: a Python  
896 toolbox for gaining geometric insights into high-dimensional data. *Journal of Machine Learning*  
897 *Research*, 18(152):1–6.
- 898 Howard, M. W. and Kahana, M. J. (2002). A distributed representation of temporal context. *Journal*  
899 *of Mathematical Psychology*, 46:269–299.
- 900 Howard, M. W., MacDonald, C. J., Tiganj, Z., Shankar, K. H., Du, Q., Hasselmo, M. E., and H., E.  
901 (2014). A unified mathematical framework for coding time, space, and sequences in the medial  
902 temporal lobe. *Journal of Neuroscience*, 34(13):4692–4707.

- 903 Howard, M. W., Viskontas, I. V., Shankar, K. H., and Fried, I. (2012). Ensembles of human MTL  
904 neurons “jump back in time” in response to a repeated stimulus. *Hippocampus*, 22:1833–1847.
- 905 Huk, A., Bonnen, K., and He, B. J. (2018). Beyond trial-based paradigms: continuous behavior, on-  
906 going neural activity, and naturalistic stimuli. *Journal of Neuroscience*, 10.1523/JNEUROSCI.1920-  
907 17.2018.
- 908 Huth, A. G., de Heer, W. A., Griffiths, T. L., Theunissen, F. E., and Gallant, J. L. (2016). Natural  
909 speech reveals the semantic maps that tile human cerebral cortex. *Nature*, 532:453–458.
- 910 Huth, A. G., Nisimoto, S., Vu, A. T., and Gallant, J. L. (2012). A continuous semantic space describes  
911 the representation of thousands of object and action categories across the human brain. *Neuron*,  
912 76(6):1210–1224.
- 913 Kahana, M. J. (1996). Associative retrieval processes in free recall. *Memory & Cognition*, 24:103–109.
- 914 Kahana, M. J. (2012). *Foundations of Human Memory*. Oxford University Press, New York, NY.
- 915 Koriat, A. and Goldsmith, M. (1994). Memory in naturalistic and laboratory contexts: distin-  
916 guishing accuracy-oriented and quantity-oriented approaches to memory assessment. *Journal of*  
917 *Experimental Psychology: General*, 123(3):297–315.
- 918 Kriegeskorte, N., Mur, M., and Bandettini, P. (2008). Representational similarity analysis – con-  
919 necting the branches of systems neuroscience. *Frontiers in Systems Neuroscience*, 2:1 – 28.
- 920 Landauer, T. K. and Dumais, S. T. (1997). A solution to Plato’s problem: the latent semantic  
921 analysis theory of acquisition, induction, and representation of knowledge. *Psychological Review*,  
922 104:211–240.
- 923 Lerner, Y., Honey, C. J., Silbert, L. J., and Hasson, U. (2011). Topographic mapping of a hierarchy  
924 of temporal receptive windows using a narrated story. *Journal of Neuroscience*, 31(8):2906–2915.
- 925 Manning, J. R. (2019). Episodic memory: mental time travel or a quantum ‘memory wave’ function?  
926 *PsyArXiv*, doi:10.31234/osf.io/6zjwb.

- 927 Manning, J. R. (2020). Context reinstatement. In Kahana, M. J. and Wagner, A. D., editors, *Handbook*  
928       of Human Memory. Oxford University Press.
- 929 Manning, J. R., Norman, K. A., and Kahana, M. J. (2015). The role of context in episodic memory.  
930       In Gazzaniga, M., editor, *The Cognitive Neurosciences, Fifth edition*, pages 557–566. MIT Press.
- 931 Manning, J. R., Polyn, S. M., Baltuch, G., Litt, B., and Kahana, M. J. (2011). Oscillatory patterns  
932       in temporal lobe reveal context reinstatement during memory search. *Proceedings of the National*  
933       *Academy of Sciences, USA*, 108(31):12893–12897.
- 934 McInnes, L., Healy, J., and Melville, J. (2018). UMAP: Uniform manifold approximation and  
935       projection for dimension reduction. *arXiv*, 1802(03426).
- 936 Mikolov, T., Chen, K., Corrado, G., and Dean, J. (2013). Efficient estimation of word representations  
937       in vector space. *arXiv*, 1301.3781.
- 938 Mueller, A., Fillion-Robin, J.-C., Boidol, R., Tian, F., Nechifor, P., yoonsubKim, Peter, Rampin, R.,  
939       Corvellec, M., Medina, J., Dai, Y., Petrushev, B., Langner, K. M., Hong, Alessio, Ozsvald, I.,  
940       vkolmakov, Jones, T., Bailey, E., Rho, V., IgorAPM, Roy, D., May, C., foobuzz, Piyush, Seong,  
941       L. K., Goey, J. V., Smith, J. S., Gus, and Mai, F. (2018). WordCloud 1.5.0: a little word cloud  
942       generator in Python. *Zenodo*, <https://zenodo.org/record/1322068#.W4tPKZNKh24>.
- 943 Murdock, B. B. (1962). The serial position effect of free recall. *Journal of Experimental Psychology*,  
944       64:482–488.
- 945 Paller, K. A. and Wagner, A. D. (2002). Observing the transformation of experience into memory.  
946       *Trends in Cognitive Sciences*, 6(2):93–102.
- 947 Pedregosa, F., Varoquaux, G., Gramfort, A., Michel, V., Thirion, B., Grisel, O., Blondel, M., Pretten-  
948       hofer, P., Weiss, R., Dubourg, V., Vanderplas, J., Passos, A., Cournapeau, D., Brucher, M., Perrot,  
949       M., and Duchesnay, E. (2011). Scikit-learn: Machine learning in Python. *Journal of Machine*  
950       *Learning Research*, 12:2825–2830.

- 951 Polyn, S. M., Norman, K. A., and Kahana, M. J. (2009). A context maintenance and retrieval model  
952 of organizational processes in free recall. *Psychological Review*, 116(1):129–156.
- 953 Postman, L. and Phillips, L. W. (1965). Short-term temporal changes in free recall. *Quarterly Journal*  
954 *of Experimental Psychology*, 17:132–138.
- 955 Rabiner, L. (1989). A tutorial on Hidden Markov Models and selected applications in speech  
956 recognition. *Proceedings of the IEEE*, 77(2):257–286.
- 957 Radford, A., Wu, J., Child, R., Luan, D., Amodei, D., and Sutskever, I. (2019). Language models are  
958 unsupervised multitask learners. *OpenAI Blog*, 1(8).
- 959 Radvansky, G. A. and Zacks, J. M. (2017). Event boundaries in memory and cognition. *Curr Opin*  
960 *Behav Sci*, 17:133–140.
- 961 Ramdas, A., Trillos, N., and Cuturi, M. (2017). On wasserstein two-sample testing and related  
962 families of nonparametric tests. *Entropy*, 19(2):47.
- 963 Ranganath, C. and Ritchey, M. (2012). Two cortical systems for memory-guided behavior. *Nature*  
964 *Reviews Neuroscience*, 13:713 – 726.
- 965 Rishel, C. A., Huang, G., and Freedman, D. J. (2013). Independent category and spatial encoding  
966 in parietal cortex. *Neuron*, 77(5):969–979.
- 967 Sigman, M. and Dehaene, S. (2008). Brain mechanisms of serial and parallel processing during  
968 dual-task performance. *Journal of Neuroscience*, 28(30):7585–7589.
- 969 Simony, E. and Chang, C. (2020). Analysis of stimulus-induced brain dynamics during naturalistic  
970 paradigms. *NeuroImage*, 216:116461.
- 971 Simony, E., Honey, C. J., Chen, J., and Hasson, U. (2016). Dynamic reconfiguration of the default  
972 mode network during narrative comprehension. *Nature Communications*, 7(12141):1–13.
- 973 Tompry, A. and Davachi, L. (2017). Consolidation promotes the emergence of representational  
974 overlap in the hippocampus and medial prefrontal cortex. *Neuron*, 96(1):228–241.

- 975 Welch, G. B. and Burnett, C. T. (1924). Is primacy a factor in association-formation. *American Journal*  
976 *of Psychology*, 35:396–401.
- 977 Yarkoni, T., Poldrack, R. A., Nichols, T. E., Van Essen, D. C., and Wager, T. D. (2011). Large-scale  
978 automated synthesis of human functional neuroimaging data. *Nature Methods*, 8(8):665.
- 979 Yonelinas, A. P. (2002). The nature of recollection and familiarity: A review of 30 years of research.  
980 *Journal of Memory and Language*, 46:441–517.
- 981 Zacks, J. M., Speer, N. K., Swallow, K. M., Braver, T. S., and Reynolds, J. R. (2007). Event perception:  
982 a mind-brain perspective. *Psychological Bulletin*, 133:273–293.
- 983 Zadbood, A., Chen, J., Leong, Y. C., Norman, K. A., and Hasson, U. (2017). How we transmit  
984 memories to other brains: Constructing shared neural representations via communication. *Cereb*  
985 *Cortex*, 27(10):4988–5000.
- 986 Zwaan, R. A. and Radvansky, G. A. (1998). Situation models in language comprehension and  
987 memory. *Psychological Bulletin*, 123(2):162 – 185.

## 988 Supporting information

989 Supporting information is available in the online version of the paper.

## 990 Acknowledgements

991 We thank Luke Chang, Janice Chen, Chris Honey, Lucy Owen, Emily Whitaker, and Kirsten Ziman  
992 for feedback and scientific discussions. We also thank Janice Chen, Yuan Chang Leong, Kenneth  
993 Norman, and Uri Hasson for sharing the data used in our study. Our work was supported in part  
994 by NSF EPSCoR Award Number 1632738. The content is solely the responsibility of the authors  
995 and does not necessarily represent the official views of our supporting organizations.

<sup>996</sup> **Author contributions**

<sup>997</sup> Conceptualization: A.C.H. and J.R.M.; Methodology: A.C.H., P.C.F. and J.R.M.; Software: A.C.H.,  
<sup>998</sup> P.C.F. and J.R.M.; Analysis: A.C.H., P.C.F. and J.R.M.; Writing, Reviewing, and Editing: A.C.H.,  
<sup>999</sup> P.C.F. and J.R.M.; Supervision: J.R.M.

<sup>1000</sup> **Author information**

<sup>1001</sup> The authors declare no competing financial interests. Correspondence and requests for materials  
<sup>1002</sup> should be addressed to J.R.M. (jeremy.r.manning@dartmouth.edu).